# Chapter-IV

Coconut husk ash fabricated CoAl-LDH composite for the enhanced sorption of malachite green dye: Isotherm, kinetics and thermodynamic studies

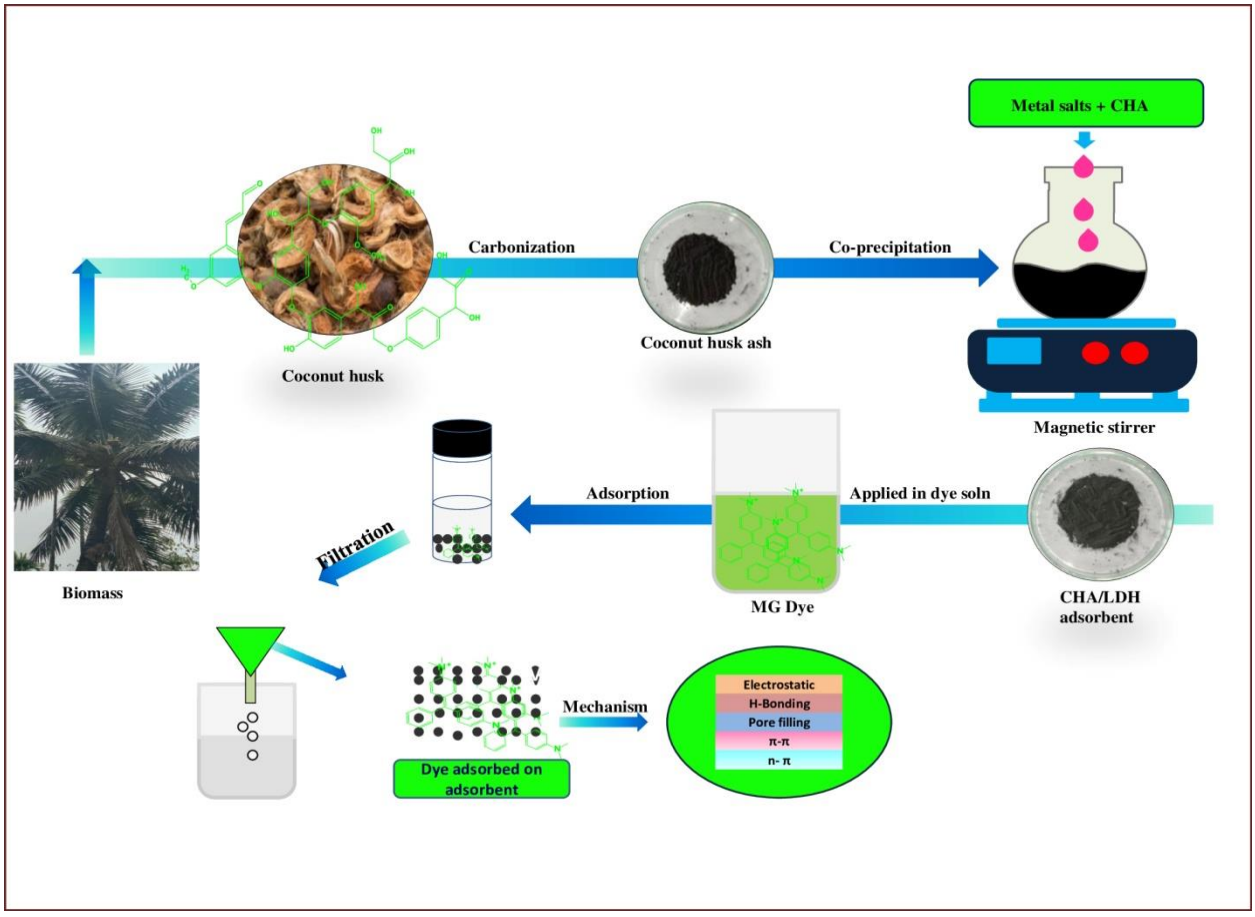

# Chapter-IV

## Coconut husk ash fabricated CoAl-LDH composite for the enhanced sorption of malachite green dye: Isotherm, kinetics and thermodynamic studies

## IV.1 Introduction

The availability of fresh and quality water has declined across the world due to the rapid advancement in manufacturing industry. Since water is a universal solvent, most of the water-soluble pollutants, either organic or inorganic, get readily dissolved in it. Consequently, the chemical properties of the safe and quality drinking water get altered due to the contaminants from various industrial discharges.[1] Among several water pollutants, the problem emerging from organic dyes are regarded as a serious issue. The ubiquitous presence of dye in the effluents discharged from various industries such as textiles, cosmetics, food, pharmaceuticals, paints, plastics, and leather is toxic, and causes severe health hazards to residential communities. These harmful effects include carcinogenic, mutagenic, heart disease, skin irritation, and allergies.[2,3] In addition, the toxicity of these organic dyes has also posed detrimental effect on the aquatic ecosystem and is of great concern. Among different cationic dyes, malachite green (MG), a triphenylmethane dye, has been extensively used for coloring wool, silk, paper, cotton, leather, and several printed products. As a result, these toxic dyes present in the form of untreated industrial wastes, when discharged freely into the natural environment, could enter the food chain and further lead to severe diseases for all living organism. [4,5] Thus, effective removal of this pollutant is very crucial in order to prevent potential hazards. Although the treatment of waste water contaminants is a major challenge, therefore investigation into the science of the interface between water pollutants and adsorbents and the development of smart material is highly urgent.

Several approaches, such as filtration, photocatalytic degradation, ozonation, oxidation, reverse osmosis, microbiological process, flocculation, and adsorption techniques were addressed for the efficient removal of organic and inorganic contaminants from the effluents. Despite the numerous methods for water remediation are available, most of these techniques encounter major drawbacks. However, the adsorption process is one of the most widely used superior treatment alternatives due to its low lost, high efficiency, eco-friendliness and simplicity.[6,7-14]

In previous works, various types of adsorbents, viz., MOF,[15,16] inorganic polymers,[17] metal oxide nanocomposite,[18,19-20] biochar,[21,22] and MXenes [23] were investigated and found capable of purifying dyes from contaminated waste water. Nevertheless, LDH was also used in water detoxification process, which are the ionic lamellar solids constituted by brucite sheets containing divalent and trivalent metal cations along with interlayer anions like $NO_3^-$, $Cl^-$, $CO_3^{2-}$, $SO_4^{2-}$. These hierarchically structured materials display attractive features such as low toxicity, high surface area, anion exchangeability, a tunable structure with various transition metal cations, and a facile synthesis method.[24] Due to their diverse applications, such as adsorption-related processes, polymer chemistry, photocatalysis, biomedicine, and electrochemistry, these materials have been extensively used as components of hybrid materials. Despite its numerous advantages, the main drawbacks of pristine LDH were it lack adequate surface functional groups and its limited use for only anionic dyes.[25,26]

Recently, the synthesis of hybrid materials between LDH and biomass derived carbon has received wide attention among researchers due to its promising sorption potential towards hazardous organic and inorganic toxins from the effluents. For instance, Zubair et al. studied the adsorption performance of date palm biochar/CuFe-LDH composite for the removal of eriochrome black T and suggested that the strong electrostatic attraction between protonated hydroxyl group of the adsorbent and $SO_3^{2-}$ anion of eriochrome black T was mainly responsible for exhibiting maximum adsorption of 565.32 mg/g.[27] Zhang et al. have reported the effective and simultaneous adsorption of inorganic nitrogen and heavy metal by MgFe/biochar composite, which is prepared by in situ loading of LDH particles over the surface of activated biochar.[28] Qu et al. investigated the removal of malachite green dye by four types of commercial activated carbon, where they advocated that the presence of strong acidic group over the adsorbent surface had negative effects on adsorption performance.[29] Meili et al. successfully synthesized a series of bovine based biochar/LDH composite as an adsorbent via the simple co-precipitation method and observed the removal of methylene blue dye from an aqueous solution with a high adsorption capacity (406.47 mg/g).[30]

During the fiscal year 2021, India was the second largest producer of coconut in the world accounting to over 14 million metric tons. It is a permanent crop, easily available and largely

supplied across different nations throughout the year. However, this massive production generates agricultural waste which can be transformed in to carbon material like charcoal and ash, otherwise left unused. Due to the great sorption capacity, high surface area, renewable nature, and high availability of these resources, further research on the development of adsorbents based on this material could be significant in the progress of water treatment technologies. Consequently, the utilization of cheap coconut husk biomass in synthesizing composite material with layered double hydroxide (LDH) can be considered a sustainable approach in the field of water remediation. Since, a large quantity of locally available feedstock, such as coconut husk, has been used only for the purposes of burning fuel and fibers, while its application in waste water treatment has not been explored. The availability of such low-cost feedstock could be utilized in preparing carbonaceous material which can act as an ideal supporting material for LDH.[31,32] Accordingly, we have adopted a suitable strategy of coupling the coconut husk derived ash with LDH to enhance their properties. The synergistic effects of LDH and coconut husk ash might widen its adsorption affinity for various water pollutants including both cationic and anionic.

Based on the detailed literature, adsorption studies of MG dye by CHA/CoAl-LDH composite was not reported. Herein, in this work we have fabricated CoAl-LDH by introducing coconut husk derived ash as a supporting material. The hybrid material CHA/CoAl-LDH was prepared via facile co-precipitation method and its dye remediation efficiency was tested for cationic dye (MG) from the aqueous solution. The as-synthesized adsorbent was characterized by various spectroscopic techniques and the effect of several experimental parameters such as temperature; pH, dosages, initial dye concentration and contact time were studied. In addition, the isotherm and kinetic modeling of the experimental data were analyzed and the possible adsorption mechanism was also demonstrated after recording the IR-spectra of MG loaded adsorbents.

## IV.2. Experimental

### IV.2.1 Materials and Methods

The coconut husk was collected from the local place Assam, India. Cobalt(II) nitrate hexahydrate ($Co(NO_3)_2.6H_2O$) (98 %) , Alumimium nitrate nonahydrate $Al(NO_3)_2.9H_2O$ (98 %), NaOH (97 %) and Malachite green ($C_{23}H_{25}ClN_2$) (98 %) was procured from Merck. The obtained chemicals

are of analytical grade and used without any further purification. The required solution in the experiment was prepared by deionised water.

### IV.2.1.1 Synthesis of CHA/CoAl-LDH Composite

The synthesis of the CHA/CoAl-LDH composite was conducted via a co-precipitation method. Initially, the collected coconut husk was heated in a muffle furnace at 300 ℃ until it was completely carbonized and transformed in to ash, which is denoted by CHA. Subsequently, 2 g of coconut husk ash (CHA) was added in 100 mL aqueous solution containing mixture of 0.1 M $Al(NO_3)_2.9H_2O$ and 0.2 M $Co(NO_3)_2.6H_2O$ metal precursors salts. The resulting mixture was allowed to agitate on a magnetic stirrer for 30 minutes. Subsequently, the alkalinity of the solution was maintained at pH 10 by adding 50 mL of 0.1 M NaOH solution in a drop wise manner, which was followed by continuous stirring the liquid suspension for 3 hours. The precipitate obtained was centrifuged and washed several times with deionised water. The resulting black slurry was then dried in an oven at 50 ℃ for 6 hours. The final product obtained was denoted as a CHA/CoAl-LDH composite.

### IV.2.1.2 Characterization

Several instrumental techniques were adopted to characterize the synthesized composites. The X-ray diffraction pattern of the adsorbents was obtained from Rigaku Ultima-IV powder X-ray diffractometer. The Cu-Kα radiation (λ = 0.154 Å, 40 KV, 30 mA) was employed as an X-ray source. The PXRD spectrum was recorded in the 2θ range from 0 to 80°. The external microstructure of the sample was observed by FE-SEM anlysis (Gemini Carl Zeiss Sigma 300). The internal morphology was discerned by using TEM (JEOL JEM-2100) under the accelerating potential of 200 KV. The FT-IR spectra of the sample were recorded by Shimadzu IR Affinity-1 by taking KBr as a reference background in the frequency range of 0-4000 $cm^{-1}$. The thermal stability of the composite was investigated with TGA (Mettlab Toledo). The specific surface area and pore volume was measured by conducting $N_2$-adsorption-desorption with the BET and BJH methods by employing the instrument Quantachrome Novawin version 11.05. For the determination of the residual dye concentration, UV-Spectrophotometer-3375 (Electronics India) was utilized. The percentage composition of the constituent elements was examined by EDX.

The point of zero charge (PZC) of the adsorbents CHA and CHA/CoAl-LDH was evaluated by using the pH drift method. During the experiment, a series of 20 mL NaCl (0.1 M) solution was poured into a conical flask, and the pH value of the solution was varied from 2-12. Eventually, 0.15 g of the adsorbents were dispersed in the solution and shaken at room temperature for a period of 24 hours. Afterwards, the suspension was filtered to separate the adsorbent, and the final pH of the supernatant liquid was measured by a digital pH meter (EI). The PZC value can be estimated from the point of intersection of the line which is obtained from the graph of pH initial vs pH final.

## IV.2.2 Adsorption Experiment

The adsorption activity of the two proposed adsorbents was investigated by applying the batch equilibrium method at a room temperature of 30 ℃. For isotherm studies, a series of malachite green dye solutions with an initial concentration (25 mg/L to 150 mg/L) was prepared in a conical flask bottle containing 20 mL each. 0.015 g of the adsorbent was dispersed in the dye solution, which was followed by agitation in a thermostatic shaker. The batches were shaken for a period of 6 hours to achieve adsorption equilibrium. Furthermore, the resulting dye solution was filtered to separate the adsorbent, and the filtrate was analyzed with UV-visible spectrophotometer to evaluate the malachite green concentration.

The amount of malachite green dye adsorbed on to the adsorbents is determined by the equation:

$$q_e = \frac{(C_0 - C_e)\,V}{W} \qquad (4.1)$$

The percentage of malachite green dye removal efficiency

$$\%\ \text{of dye removal} = \frac{(C_0 - C_e) \times 100}{C_0} \qquad (4.2)$$

where, $C_e$ and $C_0$ represents the equilibrium and initial concentration of malachite green dye solution in mg/L. $q_e$(mg/g) denotes the equilibrium adsorption capacity, $W$ and $V$ indicates quantity of adsorbent (g) and volume of the dye solution (L), respectively.

For conducting the kinetics experiments, 0.015 g of the adsorbents was mixed with 40 mL of malachite green dye solution having initial concentrations (50,100 mg/L). The dye solution is

then subjected to agitation in a thermostatic shaker, which is followed by the withdrawal of 2 mL liquid suspension after a specific time interval. Subsequently, the amount of dye adsorbed over the adsorbent was analyzed for a reaction time period of 0 to 180 minutes. Again, the adsorbent was separated from the dye solution by filtration, and its absorbance value was measured at the $\lambda_{max}$ value (655 nm) of the pollutant. The adsorption capacity at time t is evaluated by the equation:

$$q_t = \frac{(C_0 - C_t)\,V}{W} \tag{4.3}$$

where, $C_0$ and $C_t$ are the concentrations of dye at initial and at time *t*.

However, for determining the most appropriate kinetic model that can describe the sorption process, the normalized standard deviation was evaluated by the equation: [33]

$$\Delta q = \sqrt{\frac{\sum [(q_{e,exp} - q_{e,cal})/q_{exp}]^2}{N-1}} \tag{4.4}$$

where, $q_{e,cal}$ is the equilibrium sorption capacity evaluated from pseudo-first order and pseudo-second-order kinetic model, $q_{e,exp}$ is the experimental amount of adsorbate adsorbed at equilibrium, N is the number of data points.

## IV.2.2.1 Adsorption Isotherm (Langmuir)

The adsorption isotherm is an important parameter for describing the adsorbate-adsorbent interaction. It interprets the distribution of solute molecules between solid-liquid interfaces, and it is also essential for the experimental design of adsorption application in industries. Several empirical models for the adsorption isotherm were utilized to analyze the experimental data and identify the most appropriate isotherm model. The most widely used adsorption isotherm models are especially Langmuir, Freundlich, and Temkin. Based on the Langmuir model, it assumed a uniform and single-layer adsorption of the molecules over the surface of the adsorbents.[34] The linear equation for the Langmuir model is represented as:

$$\frac{1}{q_e} = \frac{1}{K_l q_m C_e} + \frac{1}{q_m} \tag{4.5}$$

where, $C_e$ denotes the equilibrium concentration of malachite green dye, $q_m$ represents maximum monolayer adsorption capacity, $K_l$ signifies the Langmuir constant which indicates the affinity between adsorbate and adsorbent, $q_e$ indicates quantity of dye adsorbed at equilibrium (mg/L).

The dimensionless separation factor for determining the feasibility of adsorption is given by the equation: [35]

$$R_L = \frac{1}{1+K_l C_o} \quad (4.6)$$

where, $C_o$ and $K_l$ signifies initial concentration of malachite green dye and Langmuir constant, respectively.

### IV.2.2.2 Freundlich

The Freundlich model is a multilayer, non uniform adsorption model that is found to be more appropriate for the heterogeneous surface of the adsorbents.[36] The linearized equation is denoted by:

$$\log q_e = \log K_f + 1/n \log C_e \quad (4.7)$$

where, $C_e$ and $q_e$ have their usual meanings, $n$ and $K_f$ are Freundlich exponents and constants, respectively. The exponent $n$ indicates the favorability or intensity of the adsorption process, while $K_f$ reveals the adsorption capacity.

### IV.2.2.3 Temkin

According to the Temkin model, the adsorption heat of all the incoming adsorbate molecules decreases linearly with the increase in the coverage of the adsorption site on adsorbent surfaces. The nature of adsorption system is characterized by the uniform arrangement of binding energy until certain maximum value.[37] The linear form of Temkin equation is described by:

$$q_e = B_T \ln A_T + B_T \ln C_e \quad (4.8)$$

where, $B_T = \frac{RT}{b_T}$, $B_T$ is related to the heat of adsorption (KJ/mol), and $A_T$ is the binding constant with respect to the maximum binding energy (L/mg), T is the temperature in Kelvin, R is the universal gas constant (8.314 J/mol.K).

## IV.2.2.4 Adsorption Kinetics

The time dependent adsorption rate and the transfer characteristic of adsorbate molecules in the adsorption system can be well understood from the kinetics studies. As a result, the kinetic parameters are very important for evaluating the adsorbent performances and also the mechanisms associated during the reaction process. The different kinetics model employed for evaluating the kinetic parameters are pseudo-first-order, pseudo-second-order, intraparticle diffusion, and the Elovich model. According to the pseudo first order model, the rate of adsorption is directly proportional to the ratio of the concentration of solutes to the amount of adsorbent.[38] The linear form of pseudo first order equation is formulated as:

$$\log (q_e - q_t) = \log q_e - \frac{K_1 t}{2.303} \qquad (4.9)$$

where, $q_t$ and $q_e$ are the quantities of dye adsorbed at time $t$ and at the equilibrium stage, respectively. The values of the rate constant $K_1$ can be evaluated from the slope of the log $(q_e - q_t)$ vs $t$ plot. On the contrary, the pseudo-second-model is based on chemisorption, where the exchange of electrons between adsorbate and adsorbent molecules occurs.[39] The linearized equation for pseudo-second-order is given as:

$$\frac{t}{q_t} = \frac{1}{K_2 q_e^2} + \frac{t}{q_e} \qquad (4.10)$$

where, $K_2$ is the pseudo-second-order rate constant, and its value is calculated from the intercept of the plot ($t/q_t$ vs $t$).

Another model proposed by Weber-Morris is the intraparticle diffusion model, which assumes that the diffusion of adsorbed molecules inside the pores of the adsorbent can also contribute in the rate-determining step of the adsorption process.[40] The equation for the intraparticle diffusion model is given by:

$$q_t = K_i\, t^{0.5} + \mathrm{I} \qquad (4.11)$$

where, $K_i$ and I are the intraparticle diffusion constant and boundary layer thickness, respectively. The values of $K_i$ and I can be determined from the slope and intercept of $q_t$ against $t^{0.5}$ plot.

## IV.2.2.5 Elovich model

To elaborate on the chemisorption nature of the adsorption system, the Elovich model was applied to the experimental kinetics data, and with the help of this model, the activation and deactivation energies of the system can be estimated. Initially, it was utilized only in gaseous system, later on, its application in solid-liquid systems is also considered valid.[41] The linearized form of Elovich equation is represented as:

$$q_t = \frac{1}{\beta} \ln(\alpha\beta) + \frac{1}{\beta} \ln(t) \qquad (4.12)$$

where, $q_t$ is the amount of malachite green dye adsorbed on CHA and CHA/LDH nanocomposite at time *t*, β indicates the extent of surface coverage (g/mg), and α denotes the initial sorption rate (mg/g.min). The magnitude of slope and intercepts obtained from the $q_t$ vs ln(*t*) plot was used for the determination of α and β values.

## IV.2.2.6 Bangham model

The Bangham kinetic model, also known as pore diffusion model, explores the influence of pore diffusions in adsorption kinetic system. To corroborate the existence of pore diffusion, the obtained kinetic data was further analyzed by the Bangham model.[42] The mathematical expression of the Bangham equation is given as:

$$\log\left[\log\left(\frac{C_o}{C_o - m q_t}\right)\right] = \log\left(\frac{K_B\, m}{2.303 V}\right) + \Delta B \log t \qquad (4.13)$$

where, m is the mass of the adsorbent (g), $q_t$ is the quantity of dye adsorbed at time *t*, and *V* indicates volume of the solution (mL), $C_o$ represents the initial dye concentration, and $K_B$ and $\Delta B$ are Bangham constants.

## IV.3. Results and Discussion

### IV.3.1 Characterization of CHA and CHA/CoAl-LDH Composite

The XRD pattern of the CHA and CHA/CoAl-LDH composite was illustrated in **Fig IV.1**. The diffraction spectrum of CHA/CoAl-LDH composite displayed characteristic peaks of pristine LDH, which are observed at the 2θ values of 11.35, 23.32, 34.28, 38.88, 46.33, 60.04 and 61.38. Moreover, the indexed plane corresponding to each observed peak was 003, 006, 012, 015, 018, 110 and 113, respectively. The obtained result is consistent with the formation of typical LDH structures, according to the previous report.[43] In addition, the peak observed in CHA at 2θ values (26.51, 38.29, 39.14, 41.29 and 58.58) was also manifested in CHA/CoAl-LDH composite, which further implies the association of carbonaceous material derived from coconut husk with the LDH structure. The appearance of sharp and intense peaks corroborates the well-defined crystalline nature of the synthesized sample. However, the peak intensity in CHA/CoAl-LDH composite decreased slightly in comparison to pristine CoAl-LDH, which might be due to the accumulation of coconut husk carbon over the crystallographic structure of LDH.[44] The lattice parameter a and c of the LDH present in composite material were evaluated by the expression $a = 2d_{110}$ and $c = 3d_{003}$, respectively. However, the determined value (a = 3 Å, c = 23.4 Å) was found almost similar to the pristine LDH. Moreover, the d-spacing value of 0.28 nm obtained from the 003 plane indicates the interlayer distance of the LDH sheet, which is not disrupted after modification with CHA material.[45]

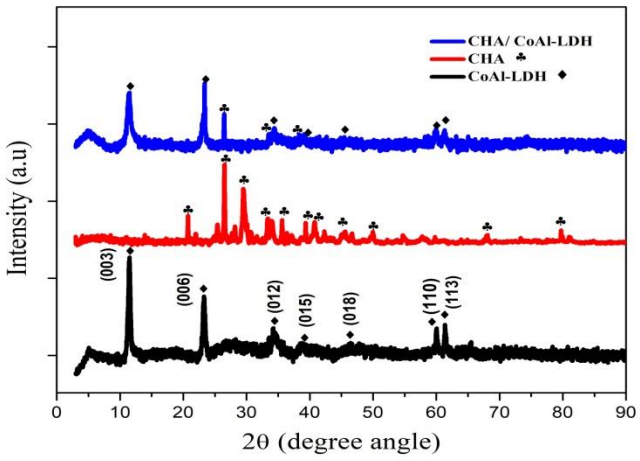


**Fig IV.1:** XRD pattern of CoAl-LDH, coconut husk ash (CHA) and CHA/CoAl-LDH composite.

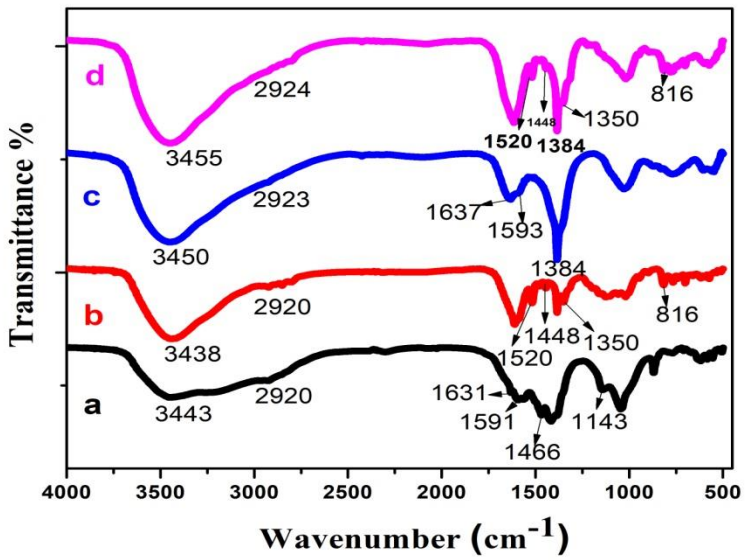


**Fig IV.2:** FT-IR spectra (a) CHA (b) CHA-MG (c) CHA/CoAl-LDH (d) CHA/CoAl-LDH-MG.

The surface functionalities of the two adsorbents, viz., CHA and CHA/CoAl-LDH composites, were elucidated by recording the FT-IR spectra, as shown in **Fig IV.2**. The respective functional groups present in CHA adsorbent (**Fig IV.2a**) were observed at the stretching frequency of 3443 $cm^{-1}$(-OH), 1631 $cm^{-1}$(C=C stretch in aromatic ring), 1591$cm^{-1}$ (conjugated C-O group of aromatic skeletal), 1466.73 $cm^{-1}$ (C-H bond), 1143 $cm^{-1}$ (C-O stretching vibration of ether, phenol, ester), and 2920 $cm^{-1}$ (C-H bond stretch).[46] After modification, in the CHA/CoAl-LDH composite (**Fig IV.2c**), the absorption peak observed at 3450 $cm^{-1}$ can be attributed to the –OH group, while the weak bands at 2923 and 2848 $cm^{-1}$ were related to the C-H stretching vibration. Another band detected at 1637 $cm^{-1}$ is also assigned due to -OH bending vibration. The stretching vibration of C-O bond and $–NO_3^-$ ion was also visible around 1593 and 1404.81 $cm^{-1}$, respectively. Moreover, the presence of M-O stretching vibration was displayed between 500 and 800 $cm^{-1}$. After analysis of FT-IR spectrum the overall results confirmed the presences of C=C, C-O, C-H, OH, and other chemical groups over the surface of CHA adsorbents. However, few functional groups were not observed in CHA/CoAl-LDH composite, which indicates the destruction in surface functional groups during the synthesis of composite material.[47,48]

The external surface morphology and the particle size of the sample CHA and CHA/CoAl-LDH composite were examined by FE-SEM analysis. **Fig IV.3(A-C)** and **3(D-F)** illustrate the FE-SEM images of CHA and fabricated CHA/CoAl-LDH composite. The micrograph of CHA depicted presences of porous structures with pore diameter lying in the range of 1 μm to 10 μm. This porous nature facilitates trapping the incoming malachite green dye molecules during the adsorption process. However, the existence of micropores and mesopores was not visible, which lie covered within the macropores. Furthermore, after fabrication of CHA with LDH, it is evident that the hexagonal platelets of LDH sheets get highly distributed over the surface of coconut husk carbon particles. Nevertheless, the relative number of macropores was also found to decrease in the composite material, which may be due to the deposition of nanosized hexagonal-shape LDH particles over the outer surface of coconut husk ash. The surface of CHA/CoAl-LDH composite (**Fig IV.3**) also revealed irregular shape, and the typical crystalline hexagonal CoAl-LDH nanoparticles were successfully assembled on the carbon matrix.[49]

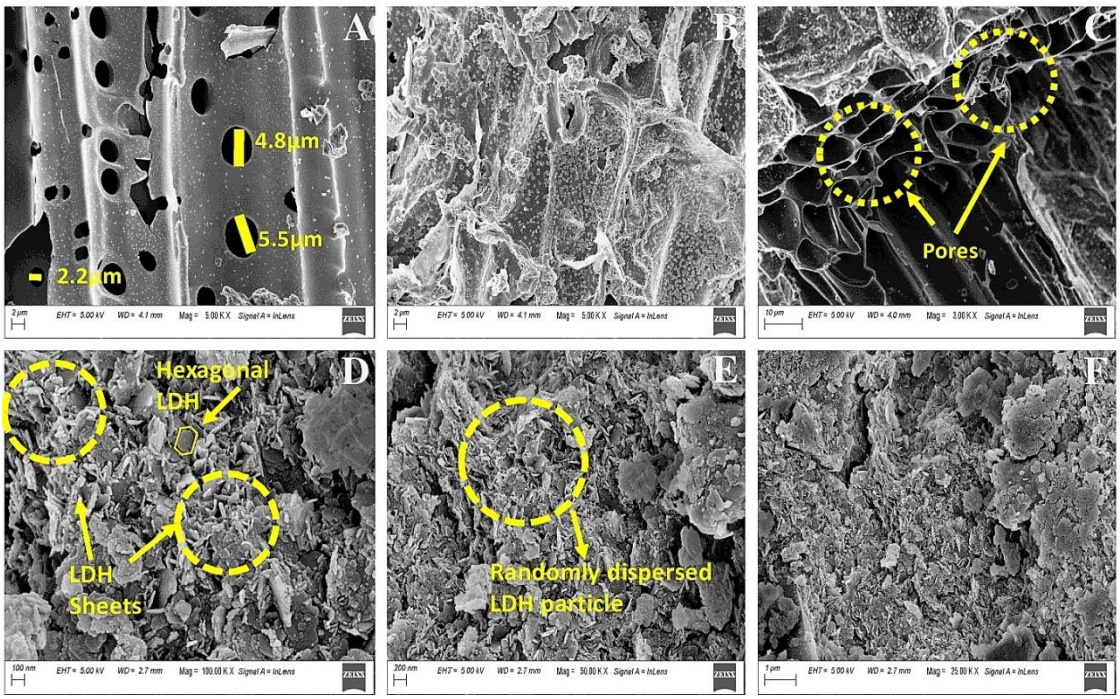


**Fig IV.3:** FE-SEM images of coconut husk ash CHA(A-C) and CHA/CoAl-LDH (D-F).

The EDX analysis of the two adsorbents, CHA and CHA/CoAl-LDH composite, was executed to determine the chemical composition and confirm the successful formation of composite materials between CoAl-LDH and CHA. **Fig IV.4(b)** shows the EDX spectra of CHA, indicating the presences of a high intense peak corresponding to C (38.55 %) and O (39.62 %) having greater weight percentage value compare to other existing elements such as Si, K, Na, Mg, P, Ca, and Cl. After fabrication of coconut husk ash with LDH, the EDX spectra (**Fig IV.4a**) of the composite material CHA/CoAl-LDH also revealed detection of all the constituent elements present in the sample CHA in addition to Co and Al. Therefore, it confirmed the formation of composite material containing both LDH phase and carbon material derived from CHA. However, the weight percentage of all the elements, including C, slightly decreased in the CHA/CoAl-LDH composite material due to the incorporation of LDH phase. In addition, the high C and O content in both CHA and CHA/CoAl-LDH composite infers the presences of acidic O-containing functional groups such as -R-OH, -OH, -C-OR, and C-C. Overall, the EDX results affirmed that a greater quantity of carbonaceous material exists in the composite material compare to the LDH phase.[50]

**Table IV.1:** The elemental composition of the proposed adsorbents CHA and CHA/CoAl-LDH determined from EDX analysis.

| **Adsorbent** | **Elemental Composition** | | | | | | | | | | |
|---|---|---|---|---|---|---|---|---|---|---|---|
| | **C%** | **O%** | **Co%** | **Al%** | **Na%** | **Mg%** | **K%** | **Ca%** | **Si%** | **Cl%** | **P%** |
| **CHA** | 38.55 | 39.62 | - | - | 2.48 | 2.66 | 5.81 | 0.90 | 5.61 | 0.35 | 0.32 |
| **CHA/CoAl-LDH** | 32.63 | 47.18 | 9.24 | 3.08 | 1.48 | 1.07 | 0.18 | 0.50 | 0.97 | 0.11 | 0.17 |

CHA = Coconut Husk Ash, LDH = Layered Double Hydroxide, EDX = Energy Dispersive X-ray

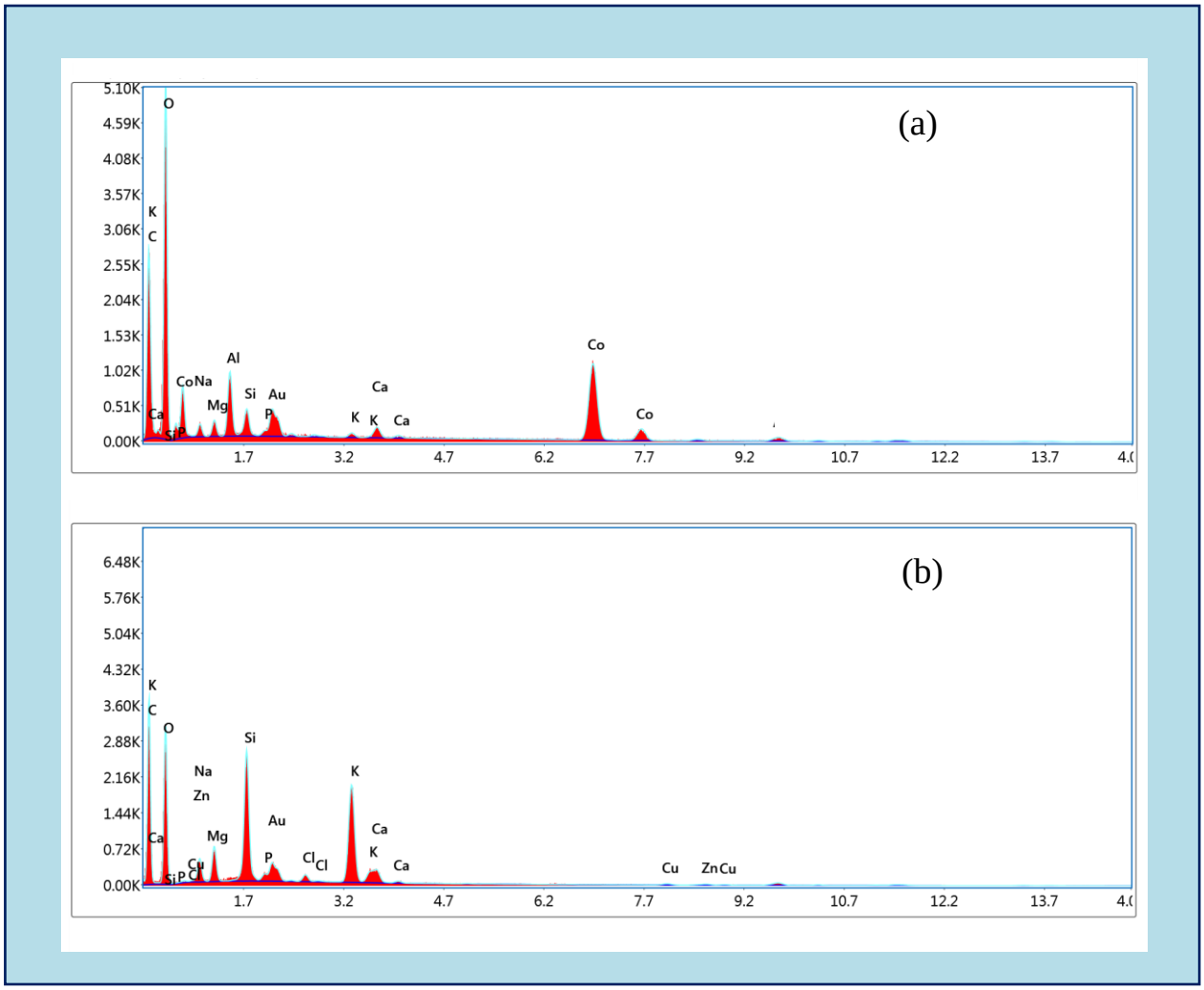


**Fig IV.4:** EDX spectra of (a) CHA/CoAl-LDH composite and (b) CHA

The size, shape, and internal morphology of the as-synthesized sample were visualized by HRTEM analysis. TEM micrographs of the adsorbent at different resolutions were depicted in **Fig IV.5 and Fig IV.6**, respectively. From **Fig IV.6**, the structure of CHA/CoAl-LDH composite also displayed aggregation of LDH particles with an average size below 100 nm, as already confirmed from SEM analysis. The heterogeneous structure of CHA/CoAl-LDH observed in **Fig IV.6(B,C)** shows that CoAl-LDH platelets was not suppressed, which further infers that the layered structure remains unaltered. However, the increasing content of coconut husk ash could lead to a significant reduction in the crystallinity of the sample. The relatively darker region spotted in **Fig IV.6(C, E)** can be attributed to the carbon material derived from CHA. In addition, the TEM images in **Fig IV.5(C,D,E)** also manifest the development of porous nature of

CHA adsorbents. The selected area electron diffraction (SAED) pattern observed in **Fig IV.5(F)** and **Fig IV.6(F)**, further corroborates the polycrystallinity of the as-synthesized sorbents.[51]

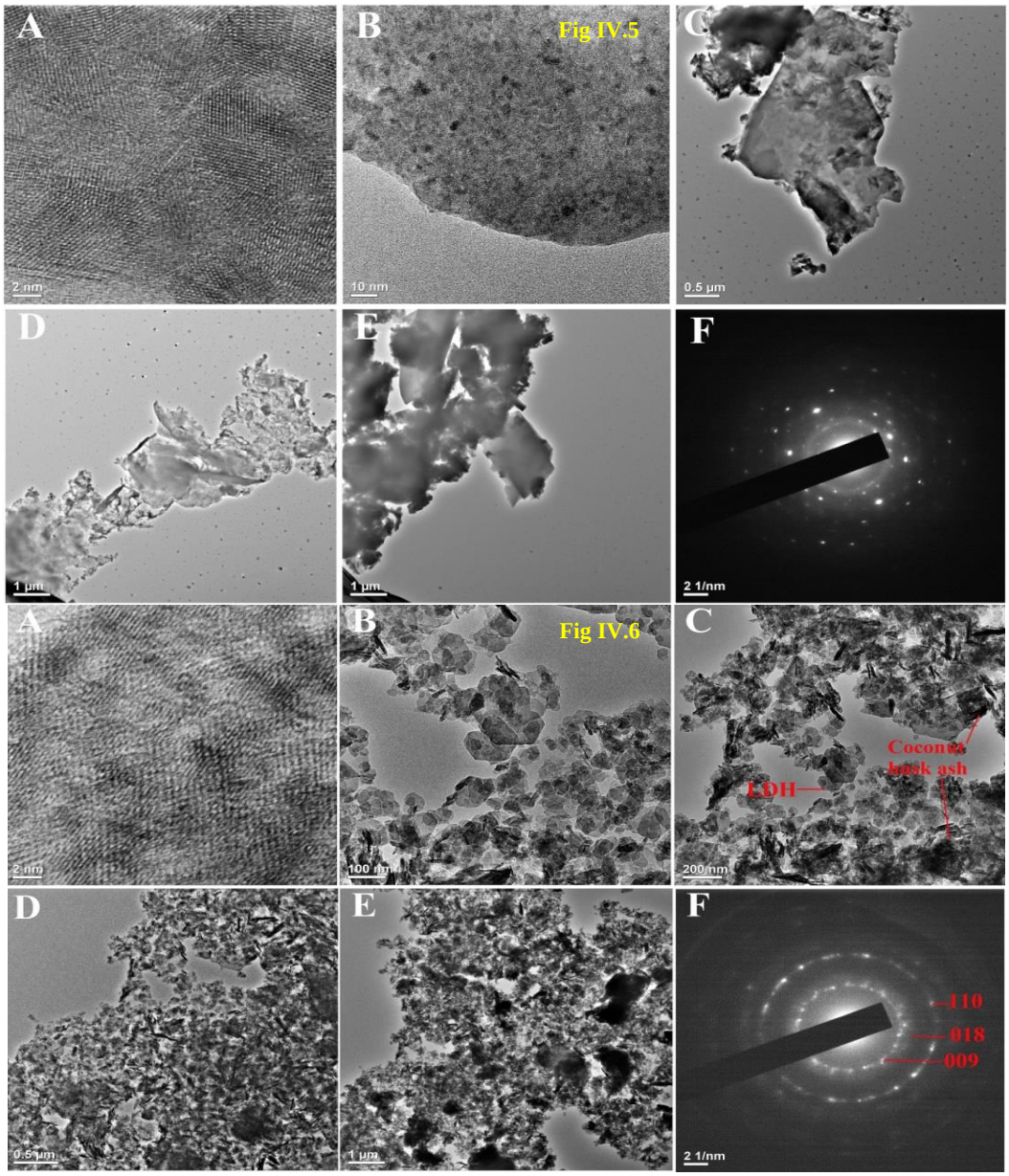


**Fig IV.5:** HRTEM images of coconut husk ash (CHA) at different magnifications (A-E) and SAED pattern (F). **Fig IV.6:** HRTEM images of CHA/CoAl-LDH at different magnification (A-E) and SAED pattern (F).

The surface properties including specific surface area, pore volume and pore size of the adsorbents CHA and CHA/CoAl-LDH composite were investigated by BET method. The porosity and specific surface area of the material is an important structural feature that can delineate characteristic information about the sorption capacity. In several cases, it was reported that an adsorbent with high specific surface area is highly preferable over low surface area due to its ability for a greater sorption capacity for organic and inorganic pollutants.[52] The $N_2$ adsorption-desorption isotherm curve of CHA and CHA/CoAl-LDH composite is depicted in **Fig IV.7(a, b)**. The insets of **Fig IV.7(a, b)** represents the pore size distribution based on the BJH method analysis. The specific surface area and pore volume of CHA (20.71 $m^2$/g, 0.051 cc/g) was relatively lower than CHA/CoAl-LDH composite (49.52 $m^2$/g, 0.202 cc/g). Despite its lower value of specific surface area and pore volume, the sorption capacity of CHA was better and showed greater $q_{max}$ value than CHA/CoAl-LDH composite. Thus, in the present studies the specific surface area of the adsorbents cannot be directly correlated in terms of adsorption capacity. Furthermore, in case of CHA **(Fig IV.7a)** the hysteresis loop is generated quickly at low relative pressure (0.127) while for CHA/CoAl-LDH composite, it initiates from higher relative pressure value (0.8). Again, from the pore size distribution curve, it is evident that porosity inside CHA adsorbent is mainly composed of mesopores which is mainly distributed between 4.01 nm to 10.17 nm.

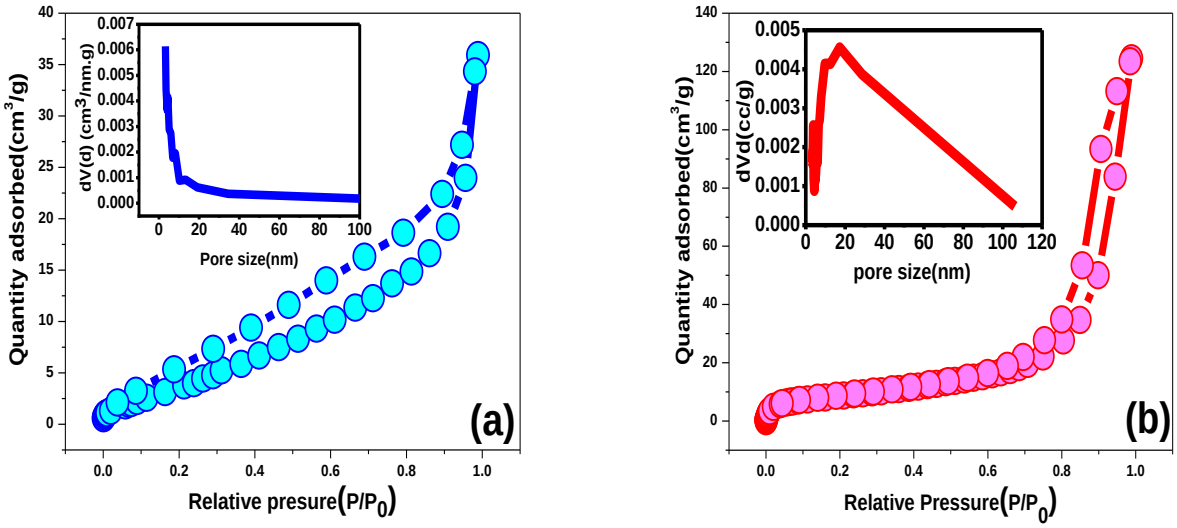


**Fig IV.7:** $N_2$ adsorption-desorption isotherm and pore sized distribution of (a) CHA and (b) CHA/CoAl-LDH composite.

Similarly, in the CHA/CoAl-LDH composite, the mesopores dominate over the micropores and the pore size lies in the range 3.88 nm to 18.32 nm. Thus, the existences of mesopores can be advantageous for the adsorption of small molecules. However, the adsorption-desorption isotherm curves of both adsorbents can be categorized under type-IV isotherms, and the hysteresis loop exhibits type-III based on IUPAC classification.[53,54]

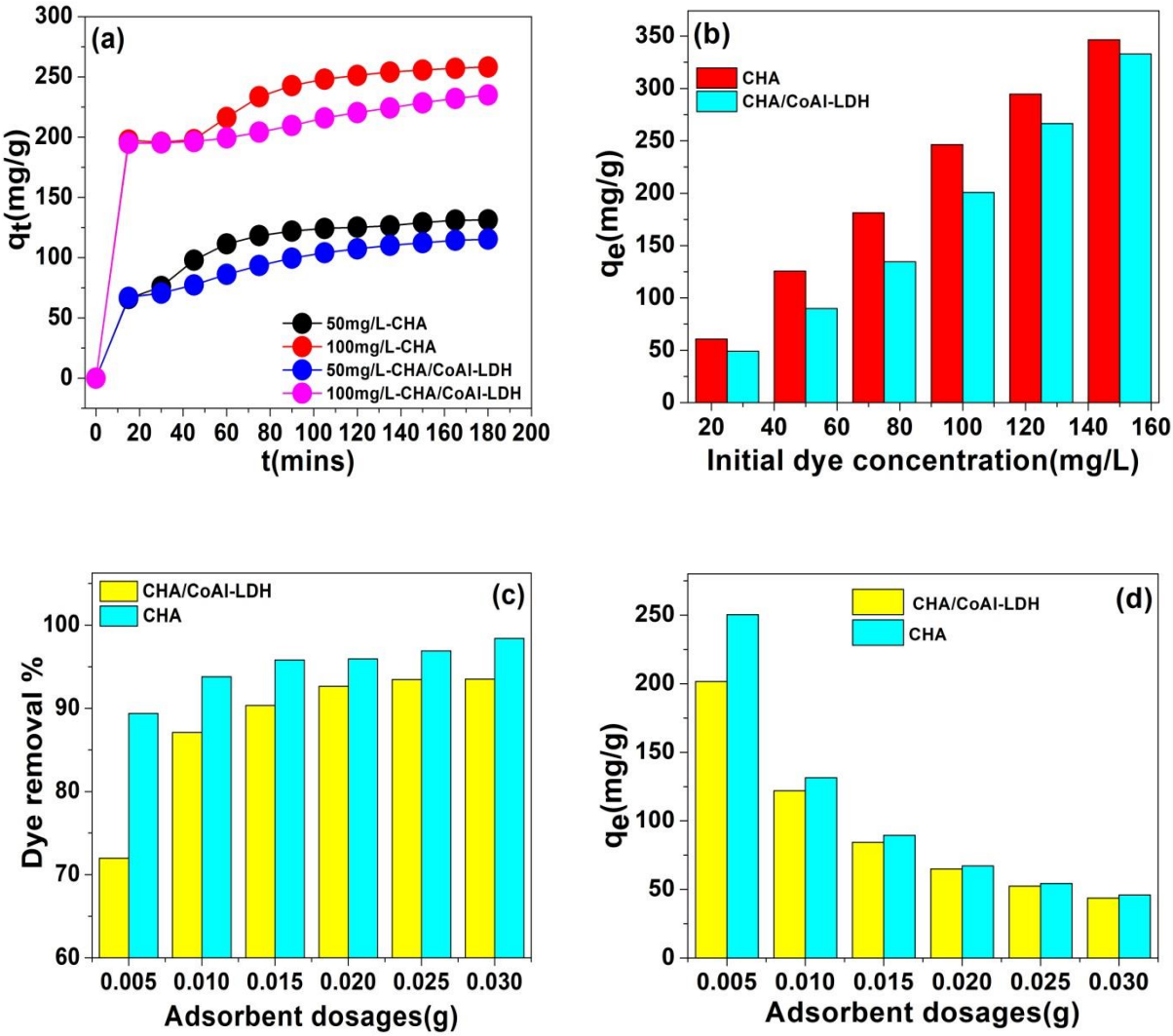


**Fig IV.8:** Effect of various parameters for adsorption of MG dye over CHA and CHA/CoAl-LDH composite (a) Contact time ($C_0$ = 50, 100 mg/L, adsorbent dosages = 0.015 g, time = 180 min, volume = 40 mL) (b) Initial dye concentration ($C_0$ = 25-150 mg/L, adsorbent dosages = 0.015 g, time = 120 min, volume = 40 mL) (c) and (d) Adsorbent dosages ($C_0$ = 70 mg/L, time = 180 min, volume=20 mL).

## IV.3.2 Effect of adsorption parameters

### IV.3.2.1 Effect of contact time

**Fig IV.8(a)** demonstrates the effect of contact time on the adsorption of malachite green dye on to the CHA and CHA/CoAl-LDH composite. The influence of contact time on the adsorption capacity of the proposed adsorbent was studied under the initial dye concentration (50, 100 mg/L) and adsorbent dosages (0.015 g). Several noteworthy results can be seen in **Fig IV.8a**, in which the $q_t$ value increases with the extension of adsorption time. At the initial stage of contact time, up to 15 minutes, the rapid adsorption rate was noticed for both adsorbents, which can be attributed to the large number of freely available adsorption sites.[55] The bending of curve between 15 and 60 min could be ascertained due to the diffusion of solute molecules inside the internal pores of the adsorbent. Subsequently, the adsorption rate slowed down due to a decrease in the active site and attained equilibrium stage after 165 minutes, where the complete coverage of the adsorption site was achieved.[56] Notably, for the studied initial adsorbate concentration (50, 100 mg/L), the maximum quantity of dye adsorbed ($q_t$) at 180 minutes for the CHA and CHA/CoAl-LDH composites were 131.38, 258.21, 115.34, and 235.09 mg/g, respectively. Since, adsorption occurred over the surface during the process, when the complete saturation of the adsorption site was attained, a steric hindrance between the incoming dye molecules and the initially adsorbed dye occurs, which led to the restriction of further dye intake. In addition, it was observed that at the fixed adsorbent dosages, the adsorption capacity of the adsorbent decreased with the increase in the molar mass of the solute molecules.[57]

### IV.3.2.2 Effect of Initial dye concentration

The effect of initial dye concentration on the adsorption capacity of CHA and CHA/CoAl-LDH composites was plotted and presented in **Fig IV.8b.** The experiment was performed under the given operating condition: ($C_o$ = 25-150 mg/L, dosages = 0.015 g, time = 120 min, volume = 40 mL). It is obvious that the equilibrium adsorption capacity increased linearly for both CHA ($q_e$ = 60.77 to 346.36 mg/L) and the CHA/CoAl-LDH composite ($q_e$ = 49.12 to 332.89 mg/L) with the increase in the initial dye concentration. In general, at constant adsorbent dosages, with an increase in dye concentration, the diffusion of solute molecules in the solution also increases.

Consequently, the physical contact of the dye molecule with the adsorbent surface occurs significantly, which can make the adsorption process more favorable. Moreover, the creation of a large concentration gradient in the adsorption site could help to overcome the mass transfer resistance of the dye molecules at the solid liquid interfaces. As a result, the adsorbent reveals greater capacity to capture dye molecules at high concentrations.[58]

### IV.3.2.3 Effect of adsorbent dosages

The quantity of adsorbent dosages added to the dye solution can affect the adsorption process. To evaluate the effect of adsorbent dosages for the removal of malachite green dye, the amount of adsorbent was varied from 0.005 to 0.03 g for both CHA and CHA/CoAl-LDH composite sorbents. The experimental condition was fixed at an initial dye concentration $C_o$ of 70 mg/L, a volume of 20 mL, and a contact time of 180 min. In **Fig IV.8c**, it is noteworthy that the percentage of dye removal increases rapidly at the adsorbent dosages of 0.005 g to 0.015 g for both adsorbents, which then slowly elevates further from 0.02 to 0.03 g. The greater percentage of dye adsorption with the increase in quantity of adsorbent can be attributed to the larger adsorption site and also to the stronger driving force.[59] However, in **Fig IV.8c**, it is apparent that there is no significant change observed in the dye removal percentage beyond 0.025 g dosages. Moreover, the equilibrium adsorption capacity $q_e$ (mg/g) in **Fig IV.8(d)** decreases from 250.32 to 45.92 mg/g for coconut husk ash (CHA), whereas in CHA/CoAl-LDH composite $q_e$ (mg/g) value get reduced from 201.56 to 43.64 mg/g with the rise in adsorbent dosages. Nevertheless, excessive use of adsorbents beyond the optimum dosages can cause the accumulation of adsorbent particles due to collision, which can further hinder the adsorption of incoming dye molecule. In addition, the maximum dye percentage for CHA (98.39 %) and CHA/CoAl-LDH (93.52 %) was achieved at 0.03 g dosages.[60]

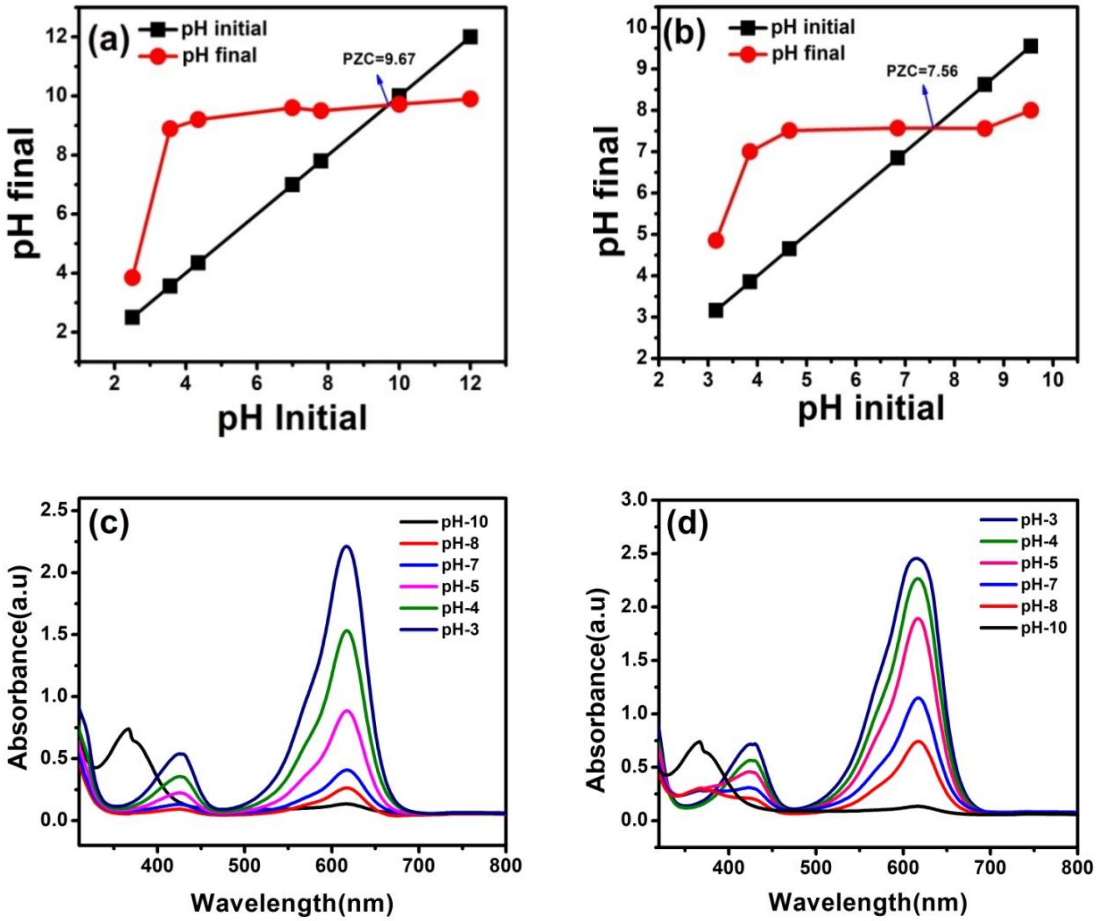


**Fig IV.9:** Determination of the point of zero charge (PZC) value of CHA/CoAl-LDH composite (a) and CHA (b) from pH initial vs pH final plot. UV-Visible spectra for the adsorption of MG dye on to CHA/CoAl-LDH composite (c) and CHA (d) adsorbents at different solution pH.

## IV.3.3.4 Effect of pH

The pH value of the aqueous solution is an essential factor to be accounted that can influence the adsorption of malachite green dye. The dye removal % of malachite green was investigated in the pH range of 3-10 at 100 mg/L MG concentration and 0.015 g adsorbent dosages. The pH of the solution can change the binding site of the adsorbent as well as the degree of ionization of the adsorbate molecule.[61] The point of zero charge value (PZC) of CHA and CHA/CoAl-LDH was determined by the pH drift method, and their respective values were obtained at 9.67 and 7.56, as in **Fig IV.9(a, b)**. In general, it is believed that at pH> PZC, the

surface charge of the adsorbent becomes negative, while at pH<PZC, it acquires +ve charge. Under an acidic medium with a low pH, the $H^+$ ions get accumulated over the surface and impart additional positive charge on the adsorbent, which causes repulsion of the cationic MG dye. Therefore, it leads to a decreased % in dye uptake. However, at higher pH under alkaline medium, dye removal % increases due to deprotonation of the surface group.[62] **Fig IV.9 (c, d)** depicts the decrease in absorbance intensity after the adsorption of MG dye on to CHA and CHA/CoAl-LDH when the pH value increases from 3 to 10.

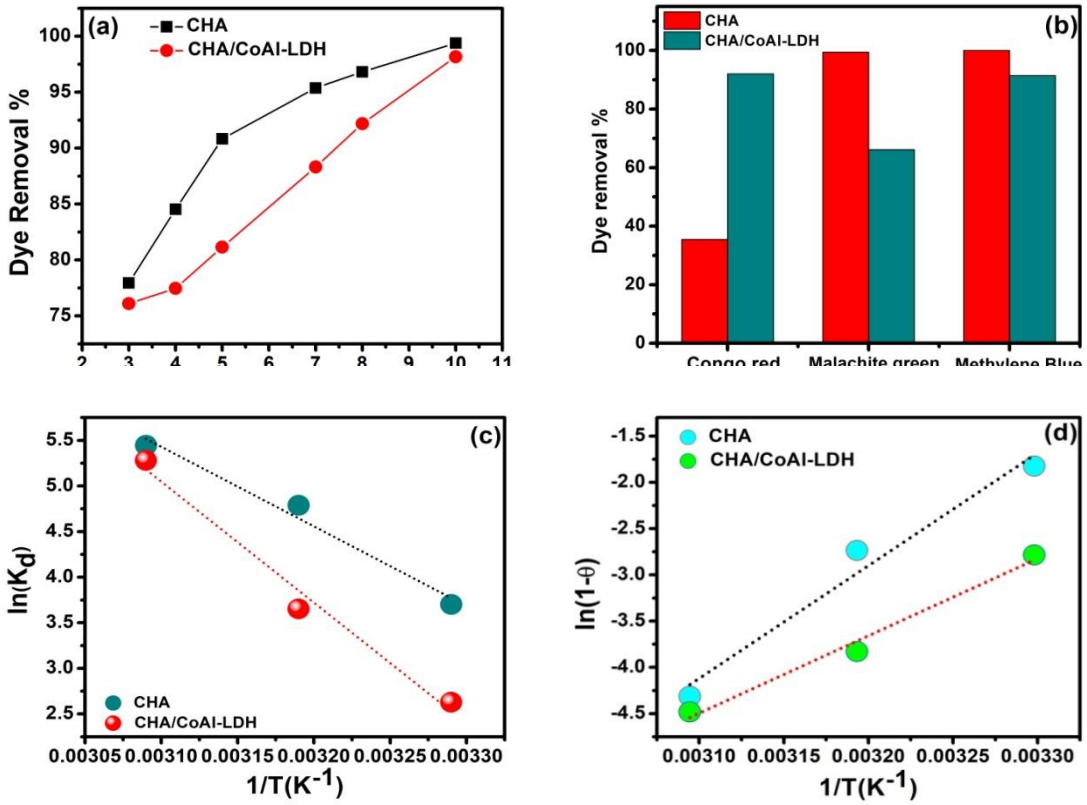


**Fig IV.10:** (a) Effect of pH on the removal percentage of MG dye ($C_0$= 100 mg/L, contact time = 120 min, dosages= 0.015 g). (b) Adsorption efficiency over various organic dyes ($C_0$ = 20 mg/L, dosages= 0.02 g, contant time = 24 hrs). (c) Vant-Hoff plot and (d) Modified Arrhenius plot for the adsorption of MG dye on to CHA and CHA/CoAl-LDH.

In CHA, the sorption efficiency increased rapidly from 77.94 to 90.83 % up to pH-5, while above pH-7, the sorption % elevated slowly from 95.38 % to 98.39 %, as shown in **Fig IV.10(a)**. Similarly, the uptake of MG dye by the CHA/LDH composite also rises with the pH value ranging from 3-10 and attained maximum adsorption of 98.16% at pH 10 towards the end of the experiment. Thus, the obtained results indicate that the variation in the pH values significantly affects the adsorption of MG dye due to the altered charged from +ve to –ve over the surface.

### IV.3.3.5 Adsorption efficiency for various organic dyes

The removal efficiency of various organic dyes on the CHA and CHA/CoAl-LDH composites was examined. **Fig IV.10(b)** clearly shows that the cationic dyes methylene blue (MB) (91.4 %) and malachite green (MG) (99.39 %) were more effectively adsorbed over CHA adsorbent than the anionic dye congo red (CR) (35.45%). However, in CHA/CoAl-LDH composite, both cationic (MG, MB) and anionic (CR) dyes are retained with the respective adsorption percentage of 91.4, 66.15, and 92 %. The lower affinity for anionic (CR) in CHA adsorbent is due to the resistance offered by negatively charged functional groups ($-COO^-$, COOR, $OH^-$) present in the adsorbent surface. On the contrary, despite having negatively charged functional sites, the existing positively charge LDH sheets and surface hydroxyl $OH^-$ in CHA/CoAl-LDH composites make them a suitable candidate for adsorption of both cationic and anionic dyes. Anionic dyes (CR) can be easily retained in CHA/CoAl-LDH composite due to the electrostatic forces and H-bonding, whereas the adsorption of cationic dyes is also attributed due to the presences of oppositely charged attraction between CHA/CoAl-LDH and dye molecules.[63] Although CHA reveal high adsorption capacity for cationic dyes, its affinity for anionic dyes was found relatively lower than that of CHA/CoAl-LDH composites.

## IV.3.4 Effect of Temperature

Thermodynamic studies were relevant to elucidate the spontaneity, adsorption mechanism, nature of adsorption, and heterogeneity of the adsorbent surface. For in-depth information about the effect of temperature on the adsorption process, the adsorption reaction was carried out at three different temperatures (303 K, 313 K, 323 K) for an initial dye concentration of 50 mg/L, with 0.015 g dosages and a contact time of 120 min. The thermodynamic nature of the present

adsorbate-adsorbent system was interpreted by evaluating various thermodynamic parameters such as Gibbs free energy (ΔG), enthalpy (ΔH), and entropy (ΔS) with the following equations:[64,65]

$$\Delta G = -RT \ln K_d \quad (4.14)$$

$$\ln K_d = \frac{\Delta S}{R} - \frac{\Delta H}{RT} \quad (4.15)$$

where, ΔG refers to Gibbs free energy, $K_d = (q_e/C_e)$ indicates adsorption distribution coefficient, T is the temperature in Kelvin and R denotes universal gas constant.

Based on the malachite green adsorption data obtained from the thermodynamic studies, the Vant-Hoff plot i.e., the linear plot of ln $K_d$ vs 1/T, was obtained. The values of the enthalpy ΔH and entropy ΔS were calculated from the slope and intercept of the plot, as shown in **Fig IV.10(c)**. **Table IV.2** summarizes the determined values of various thermodynamic parameters during the sorption experiment. It is apparent that ΔG values decreases as the temperature increases from 303 K to 323 K in both cases, which further implies the feasibility and spontaneity of adsorption process. The positive values of enthalpy change ΔH for malachite green adsorption over CHA (72.49 KJ/mol) and CHA/CoAl-LDH composite (110.24 KJ/mol) indicate the endothermic nature of adsorption. Again, the entropy changes ΔS indicate the randomness of solute molecules in the solid-liquid interface. It is obvious that the greater + ve value of ΔS in the case of the CHA/CoAl-LDH composite revealed increased randomness in the CHA/CoAl-LDH-MG interface, therefore reflecting its affinity for the dye molecules. Moreover, the obtained result shows that the adsorbent CHA has a relatively higher adsorption capacity than CHA/CoAl-LDH composite. In addition, adsorption has been found to be favored at higher temperatures, which confirms more feasibility at 323 K.

To further elucidate the dominance of either chemisorption or physisorption as the most appropriate adsorption mechanism, thermodynamic parameters such as activation energy ($E_a$) and sticking probability ($S^*$) were evaluated by applying the experimental data in modified Arrhenius equation related to surface coverage (θ). The modified Arrhenius equation is presented by the following equations:[66]

$$S^{*} = (1-\theta)\, e^{-Ea/RT} \quad (4.16)$$

$$\theta = \left(1 - \frac{C_e}{C_o}\right) \quad (4.17)$$

$$\ln S^{*} = \ln (1-\theta) - \frac{E_a}{RT} \quad (4.18)$$

$$\ln (1-\theta) = \ln S^{*} + \frac{E_a}{RT} \quad (4.19)$$

where, θ indicates surface coverage, $E_a$ (KJ/mol) denotes activation energy, $S^{*}$ represents the sticking probability, which is a temperature dependent parameter and its magnitude lies between (0-1) for a preferable process. $C_o$ and $C_e$ are the concentration of adsorbate at initial and at equilibrium, respectively.

The graphical representation of ln (1-θ) vs 1/T is displayed in **Fig IV.10(d)**. The activation energy $E_a$ and sticking probability ($S^{*}$) were calculated from the slope and intercept of the plot. In **Table IV.2**, it is clearly seen that the activation energy ($E_a$) of CHA and CHA/CoAl-LDH composite in malachite green adsorption were 101.35 and 69.50 KJ/mol, respectively. In general, the chemisorption process requires more energy, and as a result, it is associated with high activation energy ($E_a$) (40–800 KJ/mol). On the contrary, the relatively lower activation energy ($E_a$) below 40 KJ/mol is involved in the physisorption process. Since the magnitude of $E_a$ ranges between 40 and 800 KJ/mol for both adsorbents, therefore, it further corroborates chemisorption, possessing a higher potential energy barrier as the most suitable mechanism during the sorption process.[67]

**Table IV.2:** Thermodynamic parameters for the adsorption of MG dye on to CHA and CHA/CoAl-LDH composite.

| Adsorbent | T(K) | $K_d$ | ΔG(KJ/mol) | ΔH(KJ/mol) | ΔS (J/ mol. K) | $E_a$(KJ/mol) | $S^*$ |
|---|---|---|---|---|---|---|---|
| **CHA** | 303 | 3.70 | -9.36 | 72.49 | 269.87 | 101.35 | $6.4\times10^{-19}$ |
| | 313 | 4.78 | -12.46 | | | | |
| | 323 | 5.44 | -14.05 | | | | |
| **CHA/CoAl-LDH** | 303 | 2.62 | -6.62 | 110.24 | 383.71 | 69.50 | $6.23\times10^{-14}$ |
| | 313 | 3.65 | -9.50 | | | | |
| | 323 | 5.28 | -13.75 | | | | |

Initial Concentration ($C_0$) = 50 mg/L, dosages = 0.015 g, contact time = 120 min, temperature = 303 K, 313 K, 323 K, $K_d$ = adsorption distribution coefficient, ΔG = Gibbs free energy, ΔH = Enthalpy, ΔS = Entropy, S* = Sticking probability, $E_a$ = Activation energy, CHA = Coconut Husk Ash

The influence of temperature on the removal efficiency of MG onto CHA and CHA/CoAl-LDH was illustrated in **Fig IV.11**. It was observed that as the temperature elevated from 303 K to 323 K, both CHA and CHA/CoAl-LDH showed an increased in dye removal percentage. This ensures with the endothermic properties of the adsorption process. Moreover, the obtained results in thermodynamic studies also validate the suitability of the present adsorbents to be applied at high temperature reaction conditions.

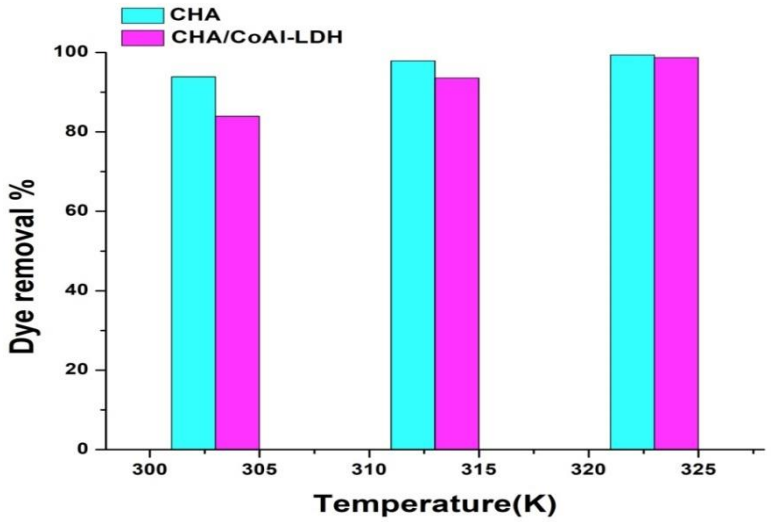


**Fig IV.11:** Effect of temperature on the removal percentage of MG dye on to CHA and CHA/CoAl-LDH. ($C_0$= 150 mg/L, contact time = 90 min, dosages = 0.015 g, volume = 40 mL)

## IV.3.5 Adsorption Isotherm

The adsorption isotherm behavior of malachite green over CHA and CHA/CoAL-LDH composite was evaluated to discern the quantitative information regarding the adsorption capacity of the adsorbent and the distribution of dye molecules between solid-liquid interfaces on reaching equilibrium. The experimental isotherm data was analyzed based on the widely used three isotherm models, namely Langmuir, Freundlich, and Temkin which is presented in **Fig IV.12** and **Table IV.3.** However, the coefficient of determination $R^2$ values for CHA and CHA/CoAl-LDH composite in Langmuir model are 0.981 and 0.993, respectively, which is relatively greater in comparison to Freundlich and Temkin model. Consequently, Langmuir model is found to be more appropriate and can best describe the experimental isotherm data. Nevertheless, it suggests that the adsorption of solute molecules takes place in a homogeneous

surface through the formation of monolayer.[68] The calculated $q_m$value obtained from the linear plot of 1/$C_e$ vs 1/ $q_e$ for CHA (943.39 mg/g), CHA/CoAl-LDH composite (666.65 mg/g) were significantly higher compare to the other adsorbents for malachite green removal.

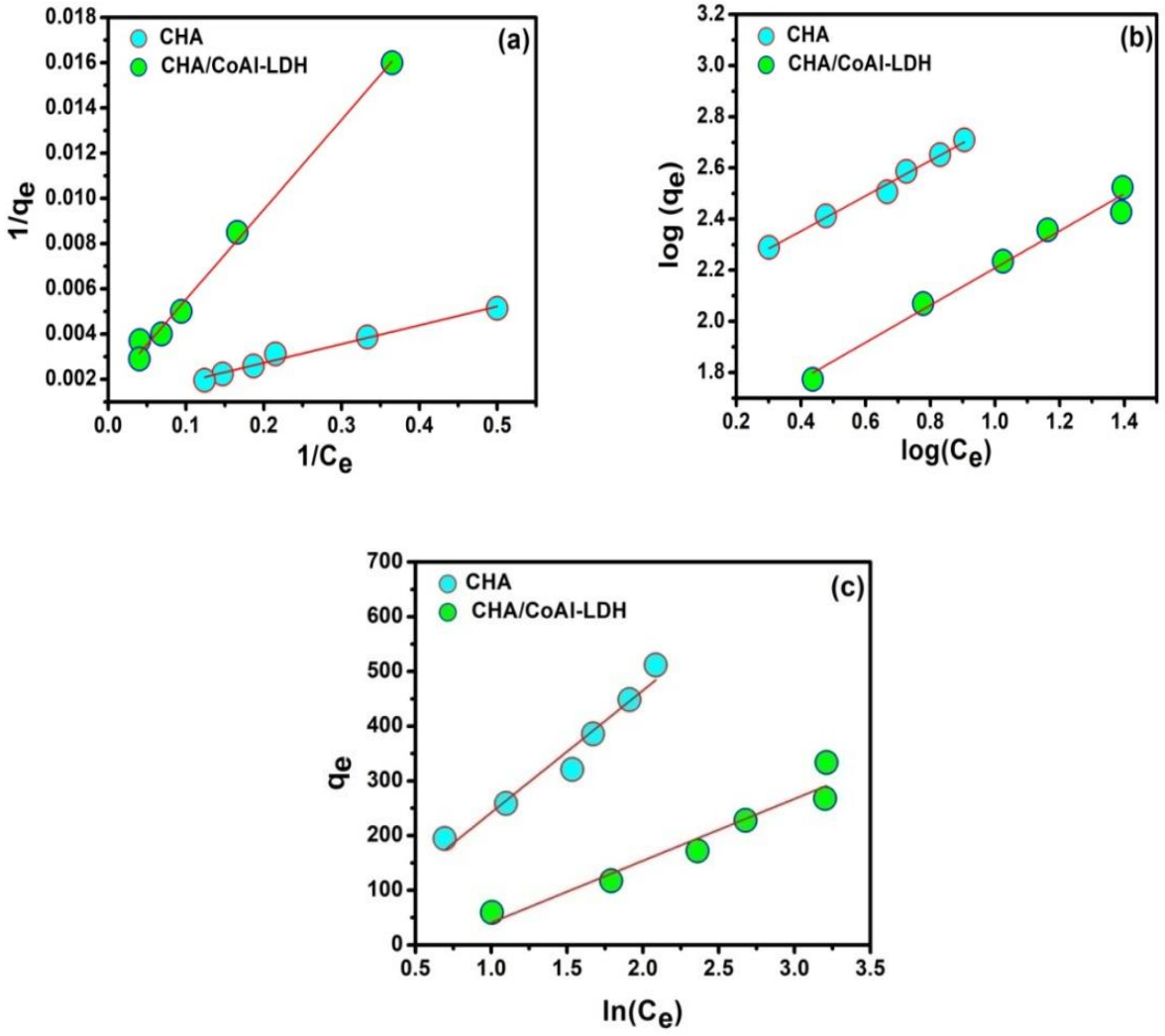


**Fig IV.12:** Linear plot of different isotherm models viz; Langmuir (a) Freundlich (b) Temkin (c) for the adsorption of MG dye on to CHA and CHA/CoAl-LDH composite.

**Table IV.3:** Langmuir, Freundlich and Temkin isotherm parameters for the adsorption of MG dye on to CHA and CHA/CoAl-LDH composite.

| **Adsorbent** | **Langmuir** | | | **Freundlich** | | | **Temkin** | | |
|---|---|---|---|---|---|---|---|---|---|
| | $q_{max}$ mg/g | $K_l$ L/mg | $R^2$ | $K_f$ (mg/g) $(L/mg)^{1/n}$ | $n$ | $R^2$ | $B_T$ | $A_T$ | $R^2$ |
| **CHA** | 943.39 | 0.12755 | 0.981 | 119.53 | 1.452 | 0.966 | 223.30 | 1.087 | 0.947 |
| **CHA/CoAl-LDH** | 666.65 | 0.03772 | 0.993 | 30.25 | 1.374 | 0.976 | 113.12 | 0.527 | 0.917 |

Initial Concentration ($C_0$ = 25-150 mg/L, volume = 20 mL, dosages = 0.015 g, time = 6 hours, $q_{max}$ = maximum monolayer capacity, $K_l$= Langmuir constant, $K_f$, n = Freundlich constant, $B_T$, $A_T$ = Temkin constant, $R^2$ = coefficient of determination, CHA = Coconut Husk Ash

The plot of $R_L$ vs $C_0$ is displayed in **Fig IV.13(a, b)**. The dimensionless separation $R_L$, which is an important parameter for elucidation of the Langmuir isotherm, is determined and lies in the range of 0-1 for both adsorbents. In general, the values of $R_L$ indicate the type of isotherm, such as irreversible ($R_L$ = 0), favorable (0<$R_L$<1), or unfavorable ($R_L$>1). Since the $R_L$ value is less than unity for both CHA and CHA/CoAl-LDH composite. Therefore, it implies a favorable intake of malachite green dye during sorption process.[69]

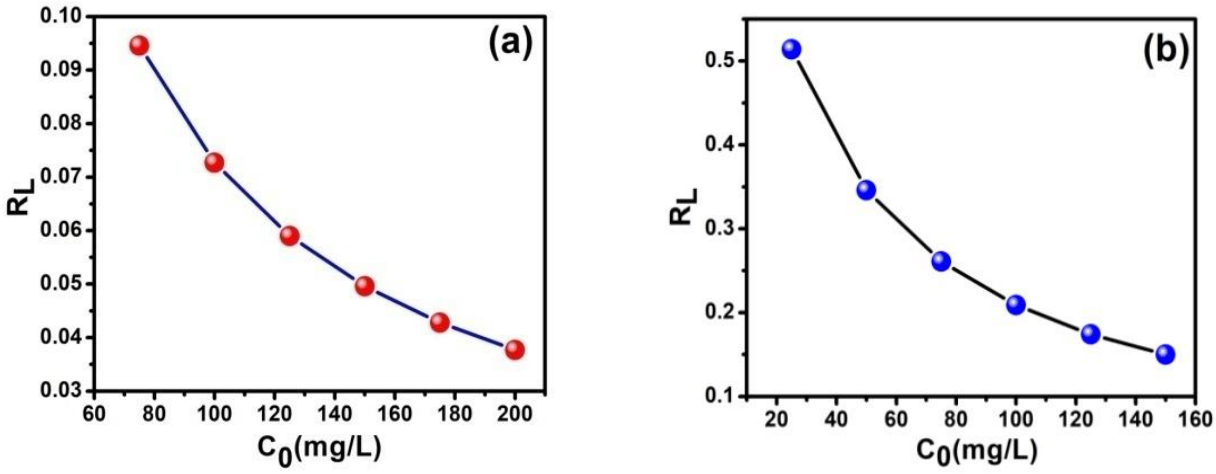


**Fig IV.13:** $R_L$ vs $C_0$ plot of (a) CHA and (b) CHA/CoAl-LDH composite.

## IV.3.6 Kinetics studies

The experimental data obtained from the kinetics studies was interpreted by pseudo-first-order, pseudo-second-order, Elovich, intraparticle diffusion, and the Bangham model, and the determined values of kinetic parameters for the adsorption of malachite green dye by two adsorbents were presented in **Table IV.4**. The linear fitting of the kinetics data based on these four models is shown in **Fig IV.14**. The coefficient of determination $R^2$ value listed in **Table IV.4** corresponding to pseudo second order model is closer to unity, and also lower normalized standard deviation Δq value was obtained compare to the first order kinetic model. Thus, it is apparent that pseudo second order model is more appropriate model for elucidating adsorption kinetics while adsorption of malachite green dye over CHA and CHA/CoAL-LDH composites. Furthermore, the rate-limiting step during the sorption process is predominantly controlled by chemisorption. In addition, the $q_e$(mg/g) values calculated from pseudo-second-order model for

CHA and CHA/CoAl-LDH composite at the initial dye concentration (50 mg/L) were 148.14 and 130.71 mg/L, respectively. The obtained values are relatively consistent with experimental $q_e$values, which are higher than the $q_{e1}$ value evaluated from pseudo-first-order model.[70]

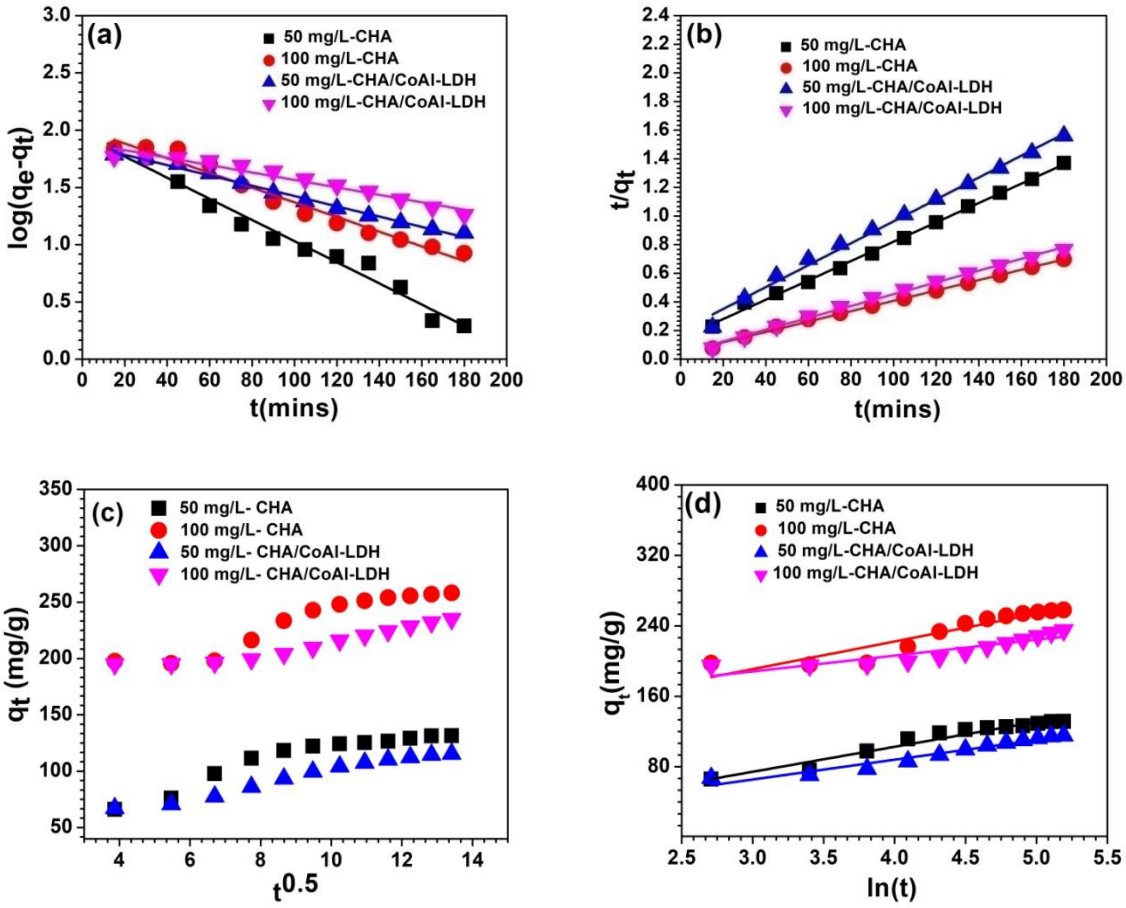


**Fig IV.14:** Linear plot of different kinetic models (a) Pseudo-first-order (b) Pseudo-second-order (c) Intraparticle diffusion (d) Elovich model.

The Weber Morris plot of $q_t$vs $t^{0.5}$ illustrated in **Fig IV.14(c**) was not a straight line passing through the origin, which confirmed that intraparticle diffusion is not the rate-limiting step in the adsorption of malachite green from an aqueous solution. The coefficient of determination $R^2$ lies between (0.86-0.97) for the entire range of contact time while fitting the kinetics data based on this model. However, it is evident that the sorption of dye takes place in three stages; initially, most of the malachite green molecules quickly occupy the vacant adsorption site present on the

external surface. In the second stage, the rate of adsorption retards due to the slow diffusion of adsorbed dye molecules inside the pore of the adsorbent. Subsequently, the equilibrium adsorption was achieved at the last stage. The thickness of boundary layer *C* corresponding to CHA and CHA/CoAl-LDH was listed in **Table IV.4**, which displayed higher value at a greater initial dye concentration. The obtained results can be described based on the increasing boundary layer effect, which is due to the rapid adsorption of vacant site by adsorbate molecules at high concentration.[71]

**Table IV.4:** Parameters of pseudo first order, pseudo second order, intraparticle diffusion and Elovich model for the adsorptive removal of MG dye by CHA and CHA/CoAl-LDH adsorbent.

| **Kinetics model** | **Parameters** | **CHA** | | **CHA/CoAl-LDH** | |
|---|---|---|---|---|---|
| | | **Dye Concentration** | | | |
| | | 50 mg/L | 100 mg/L | 50 mg/L | 100 mg/L |
| Pseudo-first order | $q_e$(exp) | 133.33 | 266.65 | 128 | 253.32 |
| | $q_{e1}$(mg/g) | 90.03 | 102.72 | 75.04 | 77.76 |
| | $K_1 \times 10^{-2}$ $min^{-1}$ | 2.12 | 1.47 | 1.03 | 0.74 |
| | $R^2$ | 0.978 | 0.964 | 0.991 | 0.951 |
| | Δq | 0.097 | 0.185 | 0.124 | 0.208 |
| Pseudo-second-order | $q_{e2}$(mg/g) | 148.14 | 276.24 | 130.71 | 242.71 |
| | $K_2 \times 10^{-4}$ ($g.mg^{-1}min^{-1}$) | 3.13 | 2.88 | 2.95 | 4.05 |
| | $R^2$ | 0.996 | 0.996 | 0.992 | 0.995 |
| | Δq | 0.033 | 0.010 | 0.006 | 0.012 |
| Intraparticle diffusion | $K_i$ ($mg/g.min^{-1}$) | 5.68 | 7.96 | 6.81 | 4.78 |
| | *C* (mg/g) | 42.80 | 158.89 | 48.94 | 167.86 |
| | $R^2$ | 0.976 | 0.905 | 0.869 | 0.919 |
| Elovich | β | 0.035 | 0.031 | 0.044 | 0.034 |
| | α | 19.40 | 693.58 | 20.74 | 953.89 |
| | $R^2$ | 0.947 | 0.872 | 0.949 | 0.793 |
| Bangham | $K_B$ | 24.92 | 51.46 | 25.31 | 59.46 |
| | $\Delta B$ | 0.294 | 0.141 | 0.254 | 0.085 |
| | $R^2$ | 0.924 | 0.870 | 0.962 | 0.805 |

The plot of $q_t$ vs ln $t$ was demonstrated in **Fig IV.14(d)**. Based on fitting the experimental kinetics data by the Elovich model, the obtained values of α were greater than β, which is summarized in **Table IV.4** for all initial dye concentrations (50, 100 mg/L). Thus, it suggests that the adsorption rate of malachite green dye on CHA and CHA/CoAl-LDH composite was comparatively higher than the desorption rate. Moreover, the coefficient of determination $R^2$ values of the linear fit were greater than 0.90 at low dye concentrations, which further validated the applicability of this model.[72]

Kinetics data were further investigated by Bangham model to identify if pore diffusion is the slowest step occurring in the adsorption kinetics experiment. The results obtained from the Bangham model are displayed in **Fig 15(a)** and **Table IV.4**. The non-linear graph was obtained from the kinetics data, which reveals that pore diffusion is not the rate-limiting step during the sorption process.[73] However, the value of coefficient of determination ($R^2$) for MG (50 mg/L) adsorption over CHA and CHA/CoAl-LDH composite adsorbent was in the range of (0.92–0.96). Although it is not significantly high enough, but it also indicates the applicability of this model to interpret the diffusion of MG dyes molecules over adsorbent surface. The determined values of $K_B$ and $\Delta B$ were CHA (0.294, 24.92) and CHA/CoAl-LDH (0.254, 25.31), respectively.

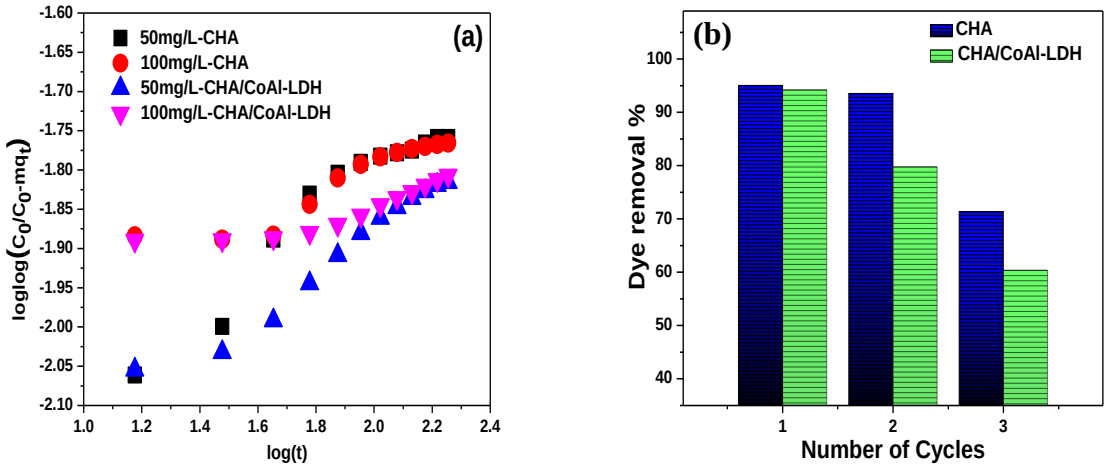


**Fig IV.15:** Graph illustrating (a) Bangham kinetic plot and (b) Reusability studies.

## IV.3.7 Adsorption Mechanism

The adsorption of MG onto CHA and the CHA/CoAL-LDH composite involves a complicated mechanism. However, the various plausible interactions associated during dye sorption are electrostatic attraction, H-bonding, π-π, n-π, ion exchange, and pore filling, which are illustrated in **Fig IV.16**. The effect of pH studies had already confirmed the influence of solution pH on the electrostatic attraction between adsorbate and adsorbent molecules. Besides, electrostatic attractions, the aromatic structure of MG dye could also be adsorbed through weak π-π and n-π interactions. The n-π and π-π interactions were initially proposed by Mattson et al. and Coughlin et al.[74,75] As depicted in **Fig IV.16**. the π-π interaction takes place between the π electrons of the negatively charged CHA or CHA/CoAl-LDH surface and the π electrons of the aromatic ring of MG. Moreover, oxygen containing functional groups such as OH, C-O can also act as electron donors, and the aromatic ring of MG can accept this electron, thereby making the n-π interaction feasible. Thus, the existence of π-π and n-π interaction can be speculated in the present studies.[76,77] However, H-bonding is another possible mechanism that can occur between OH group of the adsorbent and the electronegative elements O and N of the MG dye. The shifting of the –OH peaks in CHA (3453 to 3438 $cm^{-1}$) and CHA/CoAl-LDH composite (3447 to 3455$cm^{-1}$) can be observed from the IR-spectrum after MG adsorption, which further clarify the existences of H-bonding. Furthermore, the contribution of ion exchange and pore filling mechanism is also reported in the adsorption of cationic dye by several activated carbon and LDH/biochar composites.[78] Although the contribution of ion exchange in the current system is not clearly known, a small quantity of cations such as $K^+$, $Na^+$, and $Ca^{2+}$ present in the adsorbents CHA and CHA/CoAl-LDH may be substituted with the positively charged MG dye. Since CHA and CHA/CoAl-LDH are porous materials, as evidenced by the aforementioned BET and FE-SEM analysis, it can also be predicted that adsorption of MG dye into its non-micropore might take place via pore filling mechanisms. Additionally, after adsorption of MG dye, several new peaks were detected in between 300-1700 $cm^{-1}$ in both CHA and CHA/CoAl-LDH composite. The peak observed at stretching frequency ranging between1162-1225 $cm^{-1}$ can be attributed to the C-N stretching vibrations of the aromatic ring. In addition, the peak corresponding to C=C stretch, $CH_2$ scissoring, $CH_3$ asymmetric and $NH_2$ wag were displayed at 1520 $cm^{-1}$, 1444 $cm^{-1}$, $cm^{-1}$ and 816 $cm^{-1}$, respectively.[35] Thus, the obtained result further support

the successful adsorption of MG dye over the proposed adsorbents.

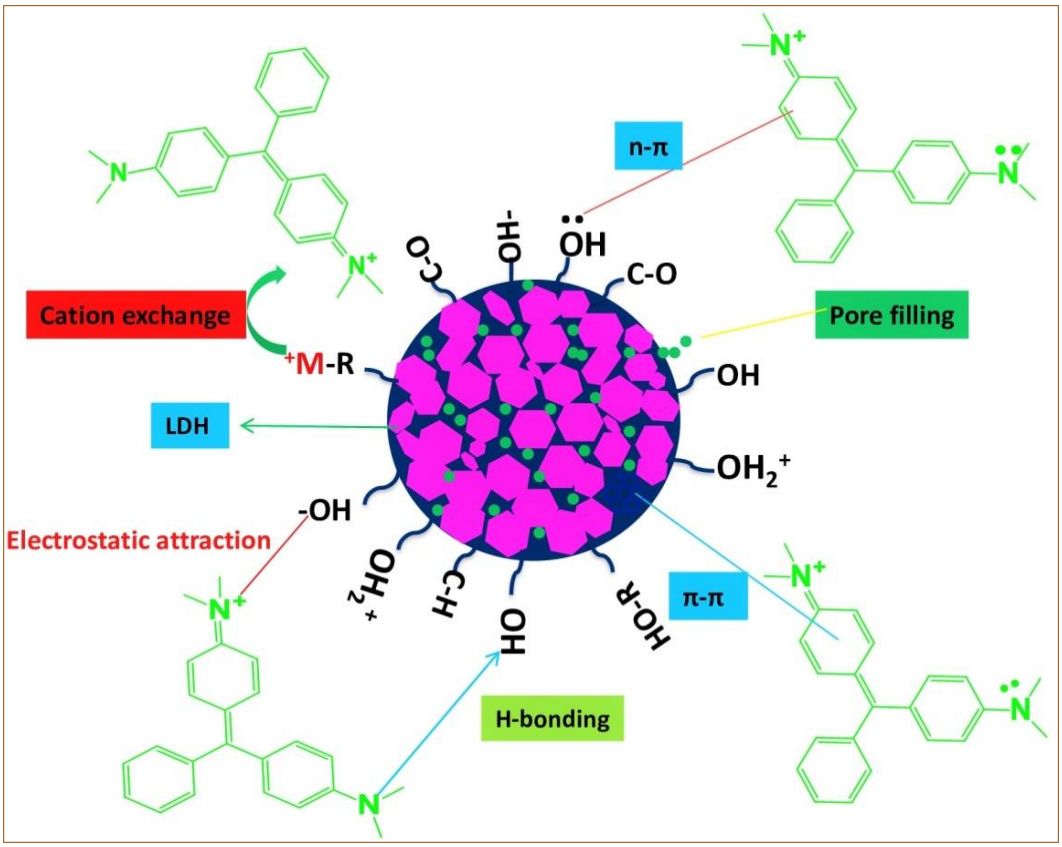


**Fig IV.16:** Plausible adsorption mechanism for adsorption of MG dye on to CHA/CoAl-LDH composite.

## IV.3.8 Comparative analysis with other adsorbents:

The maximum monolayer adsorption capacity ($q_{max}$) value of CHA and CHA/CoAl-LDH composites was compared with previously explored LDH and activated carbon to determine the potentiality of the currently studied adsorbent. From **Table IV.5**, it was observed that the adsorption capacity of CHA and the CHA/CoAl-LDH composite for MG adsorption was significantly high compare to most of the listed adsorbents. However, along with its high $q_{max}$ value, another advantage of CHA/CoAl-LDH composite was its feasibility for removing both cationic and anionic dyes.[79-87]

**Table IV.5:** Comparison of the optimum experimental condition for the adsorption of MG dye by previously reported adsorbents

| Adsorbent | pH | Dosages | Isotherm | Kinetics | $q_{max}$ (mg/g) | Ref. |
|---|---|---|---|---|---|---|
| Mn-Fe LDH/PES composite membrane | 7 | 0.02 g | Langmuir | Pseudo-second | 13.49 | [79] |
| Amygdalus Scoparia AC | 7 | 0.01 g | Langmuir | Pseudo-second | 144.30 | [80] |
| Zn Fe-LDH Nanostructure | 6 | 0.05 g | Langmuir-Freundlich | - | 71.74 | [81] |
| CuAl-$SiW_{12}O_{40}$ | - | - | Langmuir | Pseudo-second | 149.25 | [82] |
| ZIF@ZnAl-LDH | 10 | 0.01 g | Langmuir | - | 155.27 | [83] |
| NiCoAl-LDH | 10 | - | Langmuir | - | 110.13 | [84] |
| MgAl/Biochar | - | - | Freundlich | Pseudo-second | 70.92 | [85] |
| Heveabrasiliensis root AC | 4-10 | 0.2 g | n-BET | Avrami model | 259.49 | [86] |
| Coconut Husk Ash (CHA) | 10 | 0.03 g | Langmuir | Pseudo-second | 943.39 | This Work |
| CHA/LDH nanocomposite | 10 | 0.0 3 | Langmuir | Pseudo-second | 666.4 | This Work |

PES = Polyethersulfone, ZIF = Zeolitic imidazolate frameworks, AC = Activated carbon, LDH = Layered double hydroxide, $SiW_{12}O_{40}$ = Keggin type polyoxometalate, BET = Brunauer-Emmett-Teller, $q_{max}$ = Maximum monolayer adsorption capacity (mg/g)

## IV.3.9 Reusability:

The reusability test of the adsorbent is an important aspect of understanding its stability and economic feasibility for commercial and industrial applications. The reusability performance of CHA and CHA/CoAl-LDH composite was executed up to third cycle under the experimental condition fixed at $C_0$ = 60 mg/L, dosages = 0.015 g and contact time = 6 hours. After each consecutive cycle, the initially adsorbed MG dye was desorbed from the adsorbent by washing thoroughly with ethanol and distilled water. The graph of reusability test is depicted in **Fig IV. 15(b)**, it is evident that both the adsorbents showed decrease in dye removal % after each cycle. At first run, the removal capacity of MG dye by the adsorbent CHA (95%) and CHA/ CoAl-

LDH composite (94.2%) was achieved, which then slowly declines to 71.35% and 60.3%, respectively. However, this reduction in adsorption performance can occur due to the loss of the active sites during the regeneration of the adsorbents.

## IV.4 Conclusion

In summary, the composite material CHA/CoAl-LDH was successfully prepared by a facile co-precipitation method and employed for investigating its adsorptive removal of malachite green dye from the aqueous medium. SEM and TEM results indicate that CHA/CoAl-LDH as a composite exhibited porous carbon and nanosized hexagonal LDH platelets. The modification of CoAl-LDH with coconut husk ash (CHA) significantly improved the surface characteristics by enriching with several functionalities and promoted better adsorption performance towards the targeted organic pollutant. Nevertheless, the pristine CoAl-LDH does not show its adsorption affinity to cationic dye (MG) due to its inherent positively charge brucite sheets, which caused repulsion to the adsorbate molecule, while after fabrication with CHA, the maximum monolayer adsorption capacity was exceeded up to 666.4 mg/g. The effect of pH studies showed the better feasibility of CHA/CoAl-LDH in dye removal under basic pH conditions. The reusability test of the composite material indicates that after third cycle, the removal capacity drops to 60.3 %. The utilization of such a low-cost and environmentally benign carbonaceous material has produced a suitable candidate that can be exploited in multi-dye removal systems. The adsorption data has been validated well according to the Langmuir and pseudo second order models, which mainly support that the uptake of MG dye occurs through the formation of monolayer over the surface of CHA/CoAl-LDH, and also hinted the existence of chemisorption process. The probable sorption mechanism associated in CHA-MG and CHA/CoAl-LDH-MG systems resulted from several interactions, including electrostatic, H- bonding, π-π, n-π, pore filling, and ion exchange. Therefore, the present study would intrigue the new researchers in designing LDH composites by using various agricultural waste-derived carbons for the decontamination of various organic and inorganic water pollutants.

## IV. 5 References


1. B.A. Fil, *Part. Sci. Technol*., 34, **2016**, 118-126.
2. J. Khatri, P.V. Nidheesh, T.S.A. Singh, M.S. Kumar, *Chem. Eng. J*., 348, **2018**, 67-73.
3. L. D. Ardila-Leal, R. A. Poutou-Pinales, A.M. Pedroza-Rodriguez, B. E. Quevedo-Hidalgo, *Molecules*., 26, **2021**, 3813.
4. S. Srivastava, R. Sinha, D. Roy, *Aquat. Toxicol*. 66, **2004**, 319-329.
5. N. Hidayah, F.A. Bakar, N.A. Mahyudin, S. Faridah, M.S. Nur-Azura, M.Z. Zaman, *Int. Food Res. J*., 20, **2013**, 1511.
6. P. S. David, A. Karunanithi, N. N. Fathima, *Environ. Sci. Pollut. Res*., 27, **2020**, 45629-45638.
7. A.M. Saad, M. R. Abukhadra, A. K. Ahmed, A.M. Elzanaty, A.H. Mady, M.A. Betiha, J. J. Shim, A.M. Rabie, *J. Environ. Manage*., 258, **2020**, 110043.
8. M.G. Abrile, M.L. Fiasconaro, M.E. Lovato, *SN Appl. Sci*., 2, **2020**, 995.
9. V.S. Watwe, S.D. Kulkarni, P.S Kulkarni, *ACS Omega*., 6, **2021**, 27288-27296.
10. K. Ikehata, Y. Zhao, H.V. Kulkarni, Y. Li, S.A. Snyder, K.P. Ishida, M.A. Anderson, *Environ. Sci. Technol*., 52, **2018**, 8588-8595.
11. S.S. Mohanty, A. Kumar, *Sci. Rep*., 11, **2021**, 1-5.
12. M.R. Gadekar, M.M. Ahammed, *Appl. Water Sc*i. 10, **2020**, 1-8.
13. L.J. Martis, N. Parushuram, Y. Sangappa, *Environ. Sci.: Adv*., 1, **2022**, 285-296.
14. S. Moosavi, C.W. Lai, S. Gan, G. Zamini, O.A. Pivehzhani, M.R. Johan, *ACS Omega*., 5, **2020**, 20684-20697.
15. S. Yu, H. Pang, S. Huang, H. Tang, S. Wang, M. Qiu, Z. Chen, H. Yang, G. Song, D. Fu, B. Hu, X. Wang, *Sci. Total Environ*., 800, **2021**, 149662.
16. S. Zhang, J. Wang, Y. Zhang, J. Ma, L. Huang, S. Yu, L. Chen, G. Song, M. Qiu, X. Wang, *Environ. Pollut*., 291, **2021**, 118076.
17. M.E. Alouani, S. Alehyen, H.E. Hadki, H. Saufi, A. Elhalil, O.K. Kabbaj, M. Taibi, *Surf. Interfaces*., 24, **2021**, 101136.
18. M.M. Sabzehmeidani, H. Karimi, M. Ghaedi, *New J. Chem.*, 44, **2020**, 5033-5048.
19. H. Abbasi-Asl, M.M. Sabzehmeidani, M. Ghaedi, *J. Environ. Chem. Eng.* **2021**, 9, 105963.
20. M.M. Sabzehmeidani, H. Karimi, M. Ghaedi, *Arab. J. Chem.*, 13, **2020**, 7583-7597.
21. L. Liang, F. Xi, W. Tan, X. Meng, B. Hu, X. Wang, *Biochar*. 3, **2021**, 255-281.
22. A. Machrouhi, M. Farnane, A. Elhalil, R. Elmoubarki, M. Abdennouri, S. Qourzal, H. Tounsadi, N. Barka, *J. Water Reuse Desalin.*, 8, **2018**, 522-531.
23. S. Yu, H. Tang, D. Zhang, S. Wang, M. Qiu, G. Song, D. Fu, B. Hu, X. Wang, *Sci. Total Environ*., 811, **2022**, 152280.
24. R. Elmoubarki, W. Boumya, F.Z. Mahjoubi, A. Elhalil, M. Sadiq, N. Barka, *Mater. Today: Proc.*, 37, **2021**, 3871-3875.
25. J. Yu, Q. Wang, D. O´Hare, L. Sun, *Chem. Soc. Rev.* 46, **2017**, 5950-5974.
26. L. Yan, S. Gonca, G. Zhu, W. Zhang, X. Chen, *J. Mater. Chem. B*., 7, **2019**, 5583-5601.
27. M. Zubair, H. A. Aziz, I. Ihsanullah, M.A. Ahmad, M.A. Al-Harthi, *Environ. Technol. Innov.*, 23, **2021**,101614.
28. L. Zhang, S. Tang, C. Jiang, X. Jiang, Y. Guan, *ACS Appl. Mater. Interfaces*., 10, **2018**, 43013-43030.

29. W. Qu, T. Yuan, G. Yin, S. Xu, Q. Zhang, H. Su, *Fuel*., 249, **2019**, 45-53.
30. L. Meili, P.V. Lins, C.L.P.S. Zanta, J.I. Soletti, L.M.O. Ribeiro, C.B. Dornelas, T.L. Silva, M.G.A. Vieira, *Appl. Clay Sci*., 168, **2019**, 11-20.
31. L. Mishra, G. Basu, Handbook of Natural Fibres, ed. R.M. Kozlowski, M. Mackiewicz-Talarczyk, Elsevier, **2020**, vol. 1, ch. 8, pp. 231-255.
32. R.K. Ahmad, S.A. Sulaiman, S. Yusup, S.S. Dol, M. Inayat, H.A. Umar, *Ain Shams Eng. J*., 13, **2022**, 101499.
33. A. Kundu, B.S. Gupta, M.A. Hashim, G. Redzwan, *J. Clean. Prod*., 105, **2015**, 420-427.
34. I. Langmuir, *J. Am. Chem. Soc*., 40, **1918**, 1361-1403.
35. S. Das, S.K. Dash, K.M. P, *ACS Omega*., 3, **2018**, 2532-2545.
36. H.M.F. Freundlich, *J. Phys. Chem*., 57, **1906**, 385-471.
37. M.I. Temkin, *Adv. Catal.*, 28, **1979**, 173-291.
38. C.R. Lee, H.S. Kim, I.H. Jang, J.H. Im, N.G. Park, *ACS Appl. Mater. Interfaces.*, 3, **2011**, 1953-1957.
39. Y.S. Ho, G. Mckay, *Process Biochem*., 34, **1999**, 451-465.
40. W.J. Weber, J.C. Morris, *Journal of the sanitary engineering division*., 89, **1963**, 31-59.
41. F.C. Wu, R. L. Tseng, R.S. J, *Chem. Eng. J*., 150, **2009**, 366-373.
42. S. Rani, R.K. Mahajan, *Arab. J. Chem*., 9, **2016**, 1464-1477.
43. Z. Lu, W. Zhu, X. Lei, G.R. Williams, D. O′Hare, Z. Chang, X. Sun, Xue. D, *Nanoscale*., 4, **2012**, 3640-3643.
44. M.F. Anuar, Y.W. Fen, M.H.M. Zaid, K.A. Matori, R.E.M. Khaidir, *Results Phys.*, 11, **2018**, 1-4.
45. Z.P. Diao, Y.X. Zhang, X.D. Hao, Z.Q. Wen, *Ceram. Int*., 40, **2014**, 2115-2120.
46. L.Zhang, L.Y. Tu, Y. Liang, Q. Chen, Z.S. Li, C.H. Li, Z.H. Wang, W. Li, *RSC Adv.*, 8 **2018**, 42280-42291.
47. Y. Chen, C. Jing, X. Zhang, D. Jiang, X. Liu, B. D, L. Feng, S. Li, Y. Zhang, J. Colloid *Interface Sci*., 548, **2019**, 100-109.
48. O.S. Bello, K.A. Adegoka, S.O. Fagbenro, O.S. Lameed. *Appl. Water Sci*., 9 ,**2019**, 1-15.
49. L. Meili, P.V. Lins, C.L.P.S. Zanta, J.I. Soletti, L.M.O. Ribeiro, C.B. Dornelas, T.L. Silva, M.G.A. Vieira, *Appl. Clay Sci*., 168, **2019**, 11-20.
50. M.F. Anuar, Y.W. Fen, M.H.M. Zaid, K.A. Matori, R.E.M. Khaidir, *Appl. Sci*., 10, **2020**, 2128.
51. R. S. Piriya, R.M. Jayabalakrishnan, M. Maheshwari, K. Boomiraj, S. Qumabady, *Water Sci. Technol.*, 83, **2021**, 1167-1182.
52. Z. Hu, M.P. Srinivasan, *Microporous Mesoporous Mater.*, 27, **1999**, 11-18.
53. S. Kundu, M.K. Naskar, *Materials Advances*., 2, **2021**, 3600-3612.
54. H. Ma, Z. Xu, W. Wang, X. Gao, H. Ma, *RSC Adv*., 9, **2019**, 39282-39293.
55. G.Y. Abate, A.N. Alene, A.T. Habte, D.M. Getahun, *Environ. Syst. Res*., 9, **2020**, 1-13.
56. N.A. Rahmat, A.A. Ali, N. Hussain, M.S. Muhamad, R.A. Kristanti, T. Hadibarata, *Water Air Soil Pollut*., 227, 2016, 1-11.
57. N.K. Mondal, S. K, *Appl. Water Sci*., 8, **2018**, 1-12.
58. L. Ai, C. Zhang, F. Liao, Y. Wang, M. Li, L. Meng, J. Jiang, *J. Hazard. Mater*., 198, **2011**, 282-290.
59. K.G. Alpomie, F.A. Dawodu, K.O. Adebowale, *Alex. Eng. J.*, 54, **2015**, 757-767.

60. F. Ali, S. Bibi, N. Ali, Z. Ali, A. Said, Z.U. Wahab, M. Bilal, H.M.N. Iqbal, *Case Studies in Chemical and Environmental Engineering.*, 2, **2020**, 100025.
61. V.P. Dinh, T.D.T. Huynh, H.M. Le, V.D. Nguyen, V.A. Dao, N.Q. Hung, L.A. Tuyen, S. Lee, J. Yi, T.D. Nguyen, L.V. Tan, *RSC Adv*. 9, **2019**, 25847-25860.
62. I. Savva, O. Marinica, C.A. Papatryfonos, L. Vekas, T. Krasia-Christoforou, *RSC Adv*., 5, **2015**, 16484-16496.
63. G. Rathee, A. Awasthi, D. Sood, R. Tomar, R. Chandra, *Sci. Rep*., 9, **2019**, 1-14.
64. Y.T. Gebreslassie, *J. Anal. Methods Chem*., 2020, **2020**, 7384675.
65. M.A. Ahmad, R. Alrozi, *Chem. Eng. J*.,171, **2011**, 510-516.
66. V.O. Shikuku, R. Zanella, C.O. Kowenje, F.F. Donato, N.M.G. Bandeira, O.D. Prestes, *Appl. Water Sci*., 8, **2018**, 1-12.
67. J.H. Potgieter, C. Pardesi, S. Pearson, *Environ. Geochem. Health*., 43, **2021**, 2539-2550.
68. M. Maruthapandi, V.B. Kumar, J.H.T. Luong, A. Gedanken, *ACS Omega*., 3, **2018**, 7196-7203.
69. K. Sharma, H.K. Sadhanala, Y. Mastai, Z. Porat, A. Gedanken, *Langmuir*., 37, **2021**, 9927-9938.
70. E. Sterenzon, V.K. Vadivel, Y. Gerchman, T. Luxbacher, R. Narayanan, H. Mamane, *ACS Omega*., 7, **2022**, 118-128.
71. F.C. Wu, R.L. Tseng, R.S. Juang, *Chem. Eng. J*., 153, **2009**, 153, 1-8.
72. I. Ali, C. Peng, T. Ye, I. Naz, *RSC Adv*., 8, **2018**, 8878-8897.
73. A.E. Ofomaja, E.B. Naidoo, A. Pholosi, *S. Afr. J. Chem. Eng*., 32, **2020**, 39-55.
74. J.A. Mattson, H.B. Mark Jr, M.D. Malbin, W.J. Weber Jr, J.C. Crittenden, *J. Colloid Interface Sci*. 31, **1969**, 116-130.
75. R.W. Coughlin, F.S. Ezra, *Environ. Sci. Technol.*, 2, **1968**, 291-297.
76. T.G. Ambaye, M. Vaccari, E.D. V. Hullebusch, A. Amrane, S. Rtimi, *Int J Environ Sci Technol.*, 18, 2021, 3273-3294.
77. H. N. Tran, Y.F. Wang, S.J. You, H.P. Chao, *Process Saf. Environ. Prot.*, 107, **2017**, 168-180.
78. S. Fan, J. Tang, Y. Wang, H. Li, H. Zhang, J. Tang, Z. Wang, X. Li, *J. Mol. Liq.* 220, **2016**, 432-441.
79. M. Abbasi, M.M. Sabzehmeidani, M. Ghaedi, R. Jannesar, A. Shokrollahi, *Appl. Clay Sci*., 203, **2021**, 105946.
80. R. Bagheri, M. Ghaedi, A. Asfaram, E.A. Dil, H. Javadian, *Polyhedron*., 171, **2019**, 464-472.
81. R.K. Mahmoud, M. Taha, A. Zaher, R.M. Amin, *Sci. Rep*., 11, **2021**, 1-19.
82. N.R. Palapa, N. Juleanti, N. Normah, T. Taher, A. Lesbani, *Bull. Chem. React. Eng. Catal*., 15, **2020**, 653-661.
83. M.A. Nazir, M.A. Bashir, T. Najam, M.S. Javed, S. Suleman, S. Hussain, O.P. Kumar, S.S.A. Shah, *Microchem. J*., 164, **2021**, 105973.
84. M.A. Nazir, T. Najam, M.S. Bashir, M.S. Javed, M.A. Bashir, M. Imran, U. Azhar, S.S.A. Shah, A.U. Rehman, *Korean J Chem Eng*., 39, **2022**, 216-226.
85. A.F. Badri, P.M.S.B.N Siregar, N.R. Palapa, R. Mohadi, *Bull. Chem. React. Eng. Catal*., 16, **2021**, 149-160.
86. A.A. Ahmad, M.A. Ahmad, N.K.E. Yahaya, J. Karim, *Arab. J. Chem*., 14, **2021**, 103104
87. D. Brahma, H. Nath, D. Borah, M. Debnath, H. Saikia, *Inorg. Chem. Commun*., 144, **2022**, 109878.